Journal of Materials Chemistry A

ROYAL SOCIETY OF CHEMISTRY

REVIEW

View Article Online
View Journal | View Issue

Cite this: J. Mater. Chem. A, 2022, 10, 8687

Polybenzimidazoles (PBIs) and state-of-the-art PBI hollow fiber membranes for water, organic solvent and gas separations: a review

Kai Yu Wang,[a] Martin Weber[b] and Tai-Shung Chung *[ac]

Received 17th January 2022
Accepted 11th March 2022

DOI: 10.1039/d2ta00422d

rsc.li/materials-a

As an attractive candidate material, polybenzimidazole (PBI) has been explored for fabricating hollow fiber membranes (HFMs) employed in liquid and gas separations since the 1970s. Some of its membranes have achieved industrial requirements under extremely harsh process environments (*i.e.*, pH extremes, high temperatures, chlorine, organic solvents) due to its structural rigidity, robust mechanical stability, and outstanding chemical resistance. The development of high-performance industrially durable PBI HFMs is challenging owing to the complex interactions among the PBI polymer, solvents, and coagulant media during the non-solvent induced phase inversion process. State-of-the-art technologies have been developed to fabricate macrovoid-free PBI HFMs through non-solvent induced phase separation. Moreover, the chemically modified PBI membranes, PBI blended membranes and PBI composite membranes can not only improve the chemical resistance in organic solvents but also enhance the separation performance. The recently developed PBI gas separation HFMs also exhibit outstanding permselectivity and productivity exceeding the 2008 Robeson's upper bound for H_2/CO_2 separation at elevated temperatures (>200 °C). Therefore, this review aims to offer useful guidelines for researchers who are interested in PBI membranes for sustainable water and energy production. Both challenges and future opportunities of developing PBI-based HFMs will also be summarized and analyzed.

1. Introduction

Polybenzimidazoles (PBIs) are a class of heterocyclic glassy polymers that contain a benzimidazole moiety as part of the polymer repeating units. Since Vogel and Marvel initially synthesized the fully aromatic polybenzimidazoles (PBIs) from melt polycondensation of aromatic tetraamines and difunctional aromatic acids in 1961,[1] as illustrated in Fig. 1, this class of glassy heterocyclic polymers has received extensive attention due to its exceptional thermal stability, flame retardance and oxidative resistance.[2] It could exhibit remarkable thermal stability with a negligible weight loss (<5%) up to 570 °C.[3] Such unique characteristics of rigidity, high glass transition temperature (T_g of 425–436 °C) and outstanding chemical and thermal stabilities, make PBI suitable for applications in chemically challenging environments.[4–6] Many researchers had reviewed the historical development of various PBI polymers in terms of chemistry and synthesis.[7,8] The best known fully aromatic PBI is poly[2,2-(*m*-phenylene)-5,5-bibenzimidazole], also known as *meta*-PBI (*m*-PBI), commercialized by Hoechst Celanese in 1983. Today, PBI Performance Products Inc. (http://www.pbiproducts.com/) is the major provider of high performance PBI materials with the trade name of Celazole®. Comprehensive reviews of the historical development and future R & D of PBI were given by Chung in 1997 [9] and Wang *et al.* in 2016.[10] PBI-based membranes were reviewed by Cong *et al.* in 2021,[11] while PBI-based nanocomposites for advanced technical applications were given by Kausar in 2018.[12]

In the beginning, PBI was explored as a thermally stable and non-flammable textile fiber to replace asbestos,[2] and a high temperature matrix resin for aerospace and defence applications.[8] Since the heterocyclic and amphoteric benzimidazole rings in PBI molecules could not only offer superior thermal stability but also be modified by strong acids to form proton conducting membranes,[13] PBI has been extensively employed in fuel cells as polymer electrolyte membranes (PEMs) over the last 2 decades.[14–16] Specifically, after being doped with phosphoric acid or sulfuric acid, the PBI/acid complex exhibits a higher proton conductivity, lower gas permeability, and durable operation.[17–21] Wainright *et al.* first developed a PBI–phosphoric acid (PA) complex used in high-temperature fuel cells.[17] Thus, extensive studies have been devoted to PBI syntheses, modifications, membrane formation and processing as high performance, low-cost PEMs used in high-temperature fuel cells.[22–25]

[a]*Department of Chemical & Biomolecular Engineering, National University of Singapore, 4 Engineering Drive 4, 117585, Singapore. E-mail: chencts@nus.edu.sg; Fax: +65-67791936; Tel: +65-65166645*

[b]*Advanced Materials & Systems Research, BASF SE, RAP/ES-B001, 67056 Ludwigshafen, Germany*

[c]*Graduate Institute of Applied Science and Technology, National Taiwan University of Science and Technology, Taipei 106335, Taiwan*

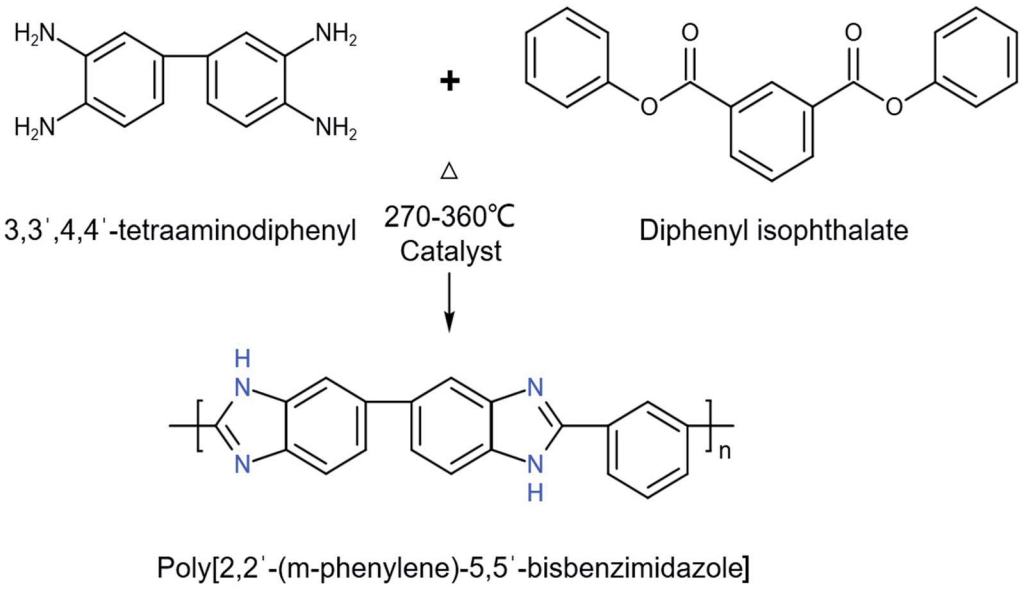

Fig. 1 Synthetic scheme of polybenzimidazole by a two-stage melt-solid polycondensation reaction.[1] (3,3′-4,4′ Tetraaminodiphenyl is also referred to as 3,3′-diaminobenzidine (DAB)).

On the other hand, PBI and quaternized-PBI can serve as a framework in forming highly anion conducting anion exchange membranes (AEMs) with outstanding alkaline resistance.[26–28] Comparing with conventional acidic fuel cells, AEM fuel cells have the most significant advantage of the much faster kinetics of the oxygen reduction reaction under alkaline operating conditions, which allows the use of non-precious metal catalysts (Ag, Ni, Co). The resultant AEM membranes can critically dominate the OH^- transport while limiting the fuel crossover. The AEMs based on quaternized-PBI/GO and quaternized-PBI/PEI blends have also been adopted in electrodialysis (ED) and membrane capacitive deionization (MCDI) for water desalination.[29,30]

Since Loeb and Sourirajan synthesized asymmetric reverse osmosis (RO) membranes from cellulose acetate *via* the phase inversion approach in the late 1950s,[31] polymeric membranes have become an attractive alternative to many energy-intensive separation processes, such as extraction, distillation, adsorption and chromatography. Systems based on pressure-driven polymer membranes become mature and accepted in many industrial separations due to their good performance, ease of scale-up, low energy consumption, environmental benignity, compact modular construction, and low operating costs compared with those thermal based systems.[32–34] Successful isothermal operations of polymeric membranes with liquids have been realized to replace and/or combine with conventional separation processes. Because of the distinguished chemical resistance, mechanical and thermal stabilities, PBI membranes have been fabricated in the geometries of flat sheets and hollow fibers for many separation applications such as microfiltration (MF) and ultrafiltration (UF), RO, nanofiltration (NF), forward osmosis (FO), pervaporation (PV), organic solvent resistant nanofiltration (OSN), and gas separation, particularly employed in aggressive environments.

Comparing with flat-sheet membranes and tubular membranes, hollow fiber membranes (HFMs) possess many inherent advantages, such as a higher surface area to volume ratio, self-supporting characteristics and a smaller footprint although the fabrication of integrally skinned HFMs with less defects is a complicated and challenging process.[34,35] This review aims to summarize (1) the developments of PBI materials including chemical modifications of PBI membranes and the variation of main chain structure during syntheses to augment their physicochemical properties and separation performance; (2) the research trends and recent development of macrovoid-free PBI HFMs fabricated by the non-solvent induced phase separation (NIPS); (3) the applications of PBI HFMs specially designed for water nanofiltration, solvent dehydration through pervaporation, organic solvent nanofiltration and H_2/CO_2 separation at elevated temperatures. Finally, the challenges and prospects of developing next-generation PBI materials and hollow fiber membranes will be discussed and analyzed.

2. The chemistry of polybenzimidazoles (PBIs)

As a member of the heterocyclic aromatic polymers, PBI is stable in common organic solvents but severe plasticization and swelling may occur when exposed to strong polar solvents, especially in polar aprotic solvents.[36] PBI can be chemically cross-linked by various compounds through covalent reactions between the N–H groups of its imidazole rings and the functionally active groups of the cross-linking agent.[37] On the other hand, modifying the PBI mainchain structure by introducing bulky groups during the polycondensation process may inhibit chain packing that can improve the gas permeability while simultaneously maintaining its high H_2/CO_2 selectivity.

2.1 Chemical crosslinking modifications of PBI membranes

Cross-linking has been considered as an efficient way to improve the chemical stability and separation performance of PBI-based membranes. Research studies that focused on the crosslinking PBI membranes are summarized below and the structures of cross-linking agents with related reaction schemes are shown in Fig. 2.

2.1.1 Green crosslinking on PBI membranes. Many studies focused on exploring green and sustainable cross-linking PBI membranes in aqueous solutions using less harmful cross-linking agents and solvents. Glutaraldehyde (GA) could be one of the green cross-linkers because this aggressive carbonyl (–CHO) reagent in aqueous solutions can still condense amines *via* Mannich reactions and/or reductive amination.[38] Xing *et al.* used GA as a bridge to connect the –NH– groups of PBI's repeating units together in an aqueous solution at room temperature.[39] Although the GA-cross-linked PBI membranes showed high fluxes of ethanol and ethyl acetate with reasonable rejections, they were unstable in harsh solvents, such as dimethylsulfoxide (DMSO). Acid-doped PBI membranes have been extensively studied in the fields of fuel cells, gas separation, pervaporation dehydration of acetic acid and OSN.[17–28,40–43] They

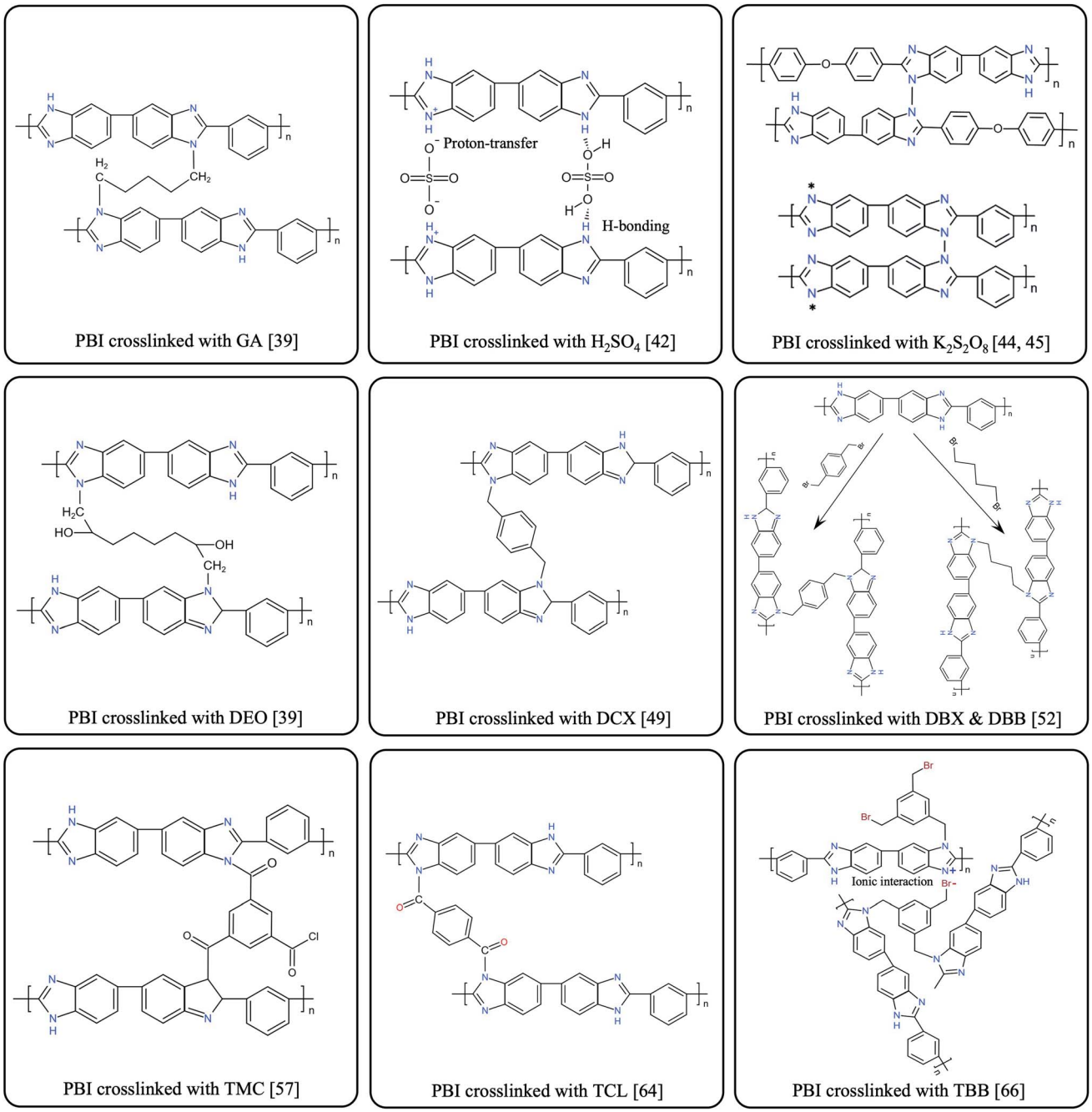

Fig. 2 Cross-linked PBI membranes with GA, H_2SO_4, $K_2S_2O_8$, DEO, DCX, DBX & DBB, TMC, TCL, TBB.

possessed excellent properties and allowed operations at high temperatures up to 200 °C without dehydration; however, low mechanical properties at high doping levels and acid leaching at extreme temperatures might occur. Chen *et al.* developed a cross-linked PBI membrane with the aid of an aqueous potassium persulphate ($K_2S_2O_8$) solution.[44] The crosslinked PBI membrane was stable in alcohols, acetone, dimethylacetamide (DMAc) and dimethylformamide (DMF) with a molecular weight cut off (MWCO) of 1000 g mol^{-1} in DMF. By employing this green cross-linking approach, Zhao *et al.* fabricated a PBI OSN HFM to separate dyes from organic solvents and regenerate the membrane by backwashing.[45]

Ignacz *et al.* presented a pioneering approach to ion-stabilize PBI and polymer of intrinsic microporosity (PIM-1) blended membranes *via* a simple HCl treatment without the use of covalent chemical crosslinking.[46] The obtained robust PBI membranes were stable in polar aprotic solvents. The incorporation of PIM-1 into the PBI membranes improved the permeance up to 4 times, and simultaneously decreased the MWCO. Hardian *et al.* developed metal–polymer coordination (MPC) solvent-resistant NF membranes owing to the superior thermal and complexation ability of benzimidazole moieties.[47] The formation of coordination bonds between the metal (copper(I) iodide, CuI) and PBI chains protected the membranes from dissolving in harsh organic solvents and improved the mechanical properties. The novel method to prepare MPC membranes provides a new route besides covalent cross-linking for the preparation of OSN membranes with tailored molecular sieving performance.

2.1.2 Covalent crosslinking on PBI membranes for OSN. When the N–H groups of PBI are attacked by 1,2,7,8-diepoxyoctane (DEO, a bifunctional epoxy), a strong bonding is formed between the N–H nucleophile and the opened epoxy group.[39] DEO-crosslinked PBI membranes exhibited extraordinary stability in polar aprotic solvents such as *N*-methyl-2-pyrrolidone (NMP), DMSO, and DMAc while having a much lower permeance. The latter may result from a reduced *d*-space between polymer chains and a decreased overall free volume due to the strong bonding between PBI and DEO. Through crosslinking PBI with epoxy-containing 3-glycidyloxypropyltrimethoxysilane (GPTMS) to form organic–inorganic siloxane networks, the robust crosslinked PBI membranes showed improved stability in harsh organic solvents such as DMF, NMP, and DMAc and a strong alkaline resistance.[48]

As reactive bifunctional alkyl halides, α,α′-dichloro-*p*-xylene (DCX), 1,4-dibromobutane (DBB) and α,α′-dibromo-*p*-xylene (DBX) can react with the –NH– groups of imidazole rings in PBI. Wang *et al.* tightened the PBI membrane structure using DCX and improved its salt rejections to separate cephalexin from aqueous solutions in NF and FO applications.[49,50] Chen *et al.* used DCX to crosslink PBI flat sheet membranes for dye rejections in organic solvent environments.[51] The DCX cross-linked PBI membranes exhibited strong tolerance (*i.e.*, minimal swelling) in tetrahydrofuran (THF) and acetone, but they were still dissolvable in DMAc and NMP. Valtcheva *et al.* developed PBI OSN membranes through cross-linking modifications with the aid of DBX and DBB.[52,53] The DBX-crosslinked PBI membrane displayed better stability in DMF and a higher solvent permeability than the DBB-crosslinked one. Both crosslinked PBI membranes were stable in extreme acidic and basic environments (pH 0 to 14). However, it was difficult to tailor the selectivity of the PBI membranes. Through the grafting modification of a long linear monoaminated polymer on the DBX-crosslinked PBI membranes, solvent stable spiral wound modules were scaled up and showed potential for industrial applications.[54]

Tashvigh *et al.* used DBX and hyperbranched polyethylenimine (HPEI) to double cross-link PBI/sulfonated polyphenylsulfone (sPPSU) blend membranes.[55] The addition of sPPSU and the double cross-linking process resulted in membranes with a higher solvent flux. The membranes had smaller pores but the permeance was not affected significantly. Tashvigh & Chung also fabricated thin film composite (TFC) membranes by forming an ultrathin and strong HPEI-DBX selective layer on top of the DBX crosslinked PBI substrate.[56] The resultant membranes not only showed good chemical stability in DMAc at 50 °C but also had an MWCO of ~350 g mol^{-1} with ethanol, acetone, THF and toluene permeances of 4.5, 14.0, 4.0 and 1.0 L m^{-2} h^{-1} bar^{-1}, respectively. Recent achievements from Prof. Szekely's group were realized through ionically crosslinking PBI with difunctional organic acids in water to improve membrane properties. The reversible nature of the PBI-based membranes enabled the successful recovery of the pristine PBI by treatment under mild basic conditions.[43]

Farahani and Chung developed a facile crosslinking approach to fabricate high-flux OSN PBI membranes by crosslinking the PBI membrane with trimesoyl chloride (TMC) in 2-methyl tetrahydrofuran (2-MeTHF) at room temperature.[57] The resultant PBI membrane had a high pure *n*-hexane permeance of 80.8 L m^{-2} h^{-1} bar^{-1} and a rejection of 90.4% to tetracycline. It also displayed stable performance in ethanol, acetone, isopropanol, and acetonitrile. As illustrated in Fig. 3, Fei *et al.* synthesized hydroxylated PBI–OH by the *N*-benzylation of PBI with 4-(chloromethyl)benzyl alcohol, blended it with graphene oxide (GO) and then covalently cross-linked the PBI/GO films with diisocyanate as mixed matrix membranes (MMMs).[58] It was found that the anchored GO could stabilize the polymer matrix through robust π–π interactions with the modified PBI polymer chains.[59] The PBI/GO membranes not only showed high permeances in high polarity solvents but also had a high rejection > 93% for a solute with a molecular weight of 420 g mol^{-1} in both polar and nonpolar solvents, such as acetone, THF, acetonitrile (MeCN), dichloromethane (DCM), and DMF. Zhao *et al.* fabricated robust PBI composite membranes through encapsulating a dopamine monomer in the PBI membrane matrix by NIPS, followed by *in situ* polymerization of dopamine initiated with $NaIO_4$ to form an interpenetrating polymer network (IPN),[60] as shown in Fig. 4. Although both FTIR and solid-state NMR analyses did not detect the occurrence of covalent cross-linking modifications, the membrane displayed solvent stability in seven polar aprotic solvents up to 100 °C due to the combined effects from the strong secondary interaction between PBI and polydopamine (PDA), and the formation of IPN. A permeance up to 12 L m^{-2} h^{-1} bar^{-1} in DMF was obtained with a MWCO of

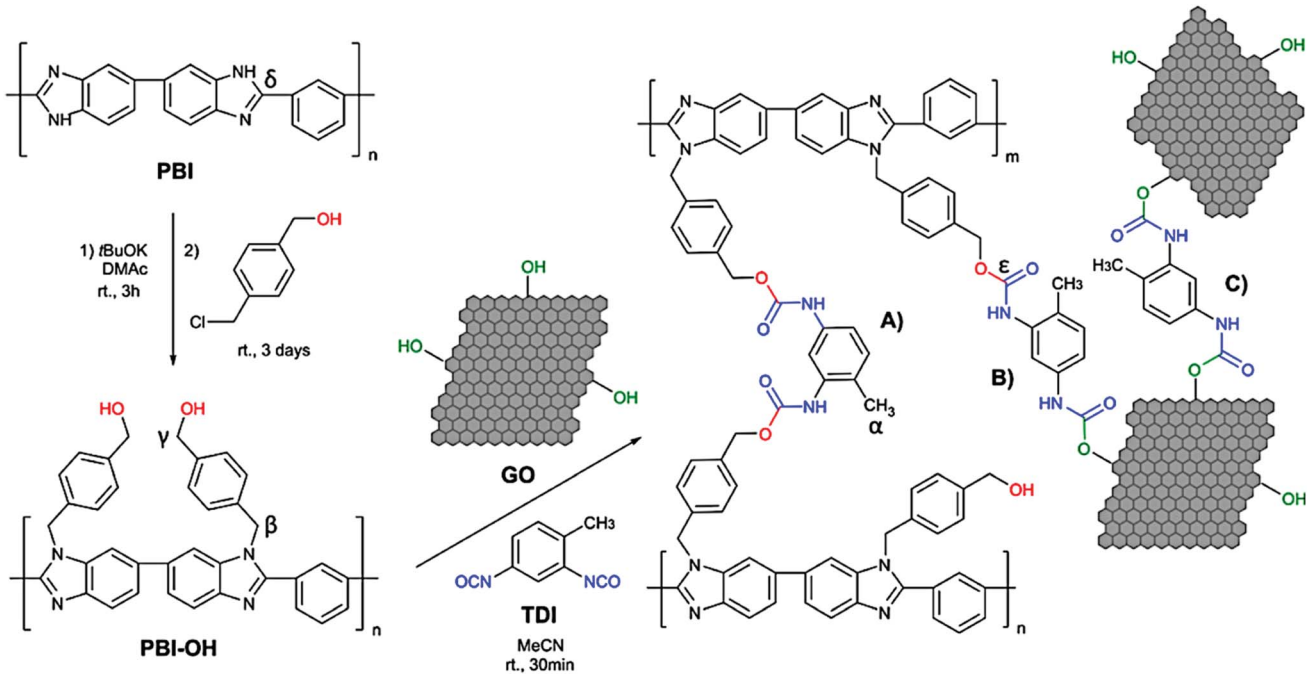

Fig. 3 Reaction scheme showing the *N*-benzylation of polybenzimidazole and the diisocyanate-based (A) cross-linking of hydroxylated polybenzimidazole chains, (B) anchoring of GO sheets, and (C) cross-linking of GO sheets. Reproduced with permission from ref. 58, copyright 2018, ACS Publications.

190–850 g mol^{-1}. PDA can also be used as a functional layer for an additional coating or as a selective layer by various cross-linking approaches. Fei *et al.* reported a pioneering study by using an oxidant-promoted biophenol coating as a versatile, reproducible, and easily scalable method to finely tailor the separation performance of PBI OSN membranes.[61] Kim *et al.* developed a robust and tight PBI-based OSN membranes through reinforcing the active layer with an ultrathin PDA coating followed by the simultaneous co-crosslinking of the PDA-coated PBI membranes.[62] The PDA layer can effectively improve the pristine PBI membrane performance by reducing the overall pore size and filling the defects at the PBI membrane surface. PDA coated PBI/GO composite membranes for oil-in-water emulsion separation demonstrated promising long-term antifouling and antimicrobial properties.[63]

2.1.3 Covalent crosslinking on PBI membranes for gas separation. For gas separation, cross-linking generally results in a higher selectivity but a lower permeability for H_2/CO_2 gas separation due to the reduced *d*-space and fractional free volume (FFV) between molecular chains. Zhu *et al.* proposed a facile cross-linking method of fabricating PBI thin films where the acyl chloride groups of terephthaloyl chloride (TCL) reacted with the –NH– groups in imidazole rings of PBI to form tertiary amide groups.[64] The cross-linking modification could severely reduce CO_2 sorption but only slightly reduce H_2 permeability, thus it significantly increased the H_2/CO_2 selectivity. The resultant PBI thin films surpassed the 2008 Robeson's upper bound estimated at 200 °C (ref. 65) and displayed a H_2 permeability of 39 barrer and a H_2/CO_2 selectivity of 23 using a mixed gas of 50/50 (v/v) H_2/CO_2 as the feed. Naderi *et al.* crosslinked PBI membranes with the aid of 1,3,5-tris(bromomethyl)benzene (TBB) to enhance the sieving ability by reducing *d*-spacing and FFV.[66] The TBB-crosslinked PBI membranes showed high thermal stability up to 560 °C and a greater decline in CO_2 diffusivity than solubility, which resulted in a higher H_2/CO_2 diffusivity selectivity. Under mixed gas tests of 50/50 (v/v) H_2/CO_2, the TBB-crosslinked PBI membrane had a H_2 permeability of 9.6 barrer and a H_2/CO_2 selectivity of 24 at 150 °C above the 2008 Robeson's upper bound. Hosseini *et al.* cross-linked the PBI/Matrimid blend membranes using DCX and *p*-xylene diamine (XDA) separately.[67] The cross-linked PBI/Matrimid (75/25 wt%) membrane with XDA exhibited a better H_2/CO_2 selectivity of around 26 owing to the reduced segment mobility of polymer chains and the increased chain packing density.

Two-dimensional (2D) materials such as graphene oxides (GOs), MoS_2, and MXene can be made into a laminar membrane through stacking 2D single layers with sub-nanometer channels that serve as molecular sieves to separate small gas molecules (*i.e.*, H_2 or He) from large gas molecules (*i.e.*, N_2, CO_2, and CH_4).[68–70] Jin *et al.* developed a cross-linked PBI-triglycidylisocyanurate (TGIC) and 2-D sulfonated graphene (SG) composite membrane with a thickness of 132 μm.[70] It could separate H_2 from CO_2 based on the mixed proton–electron conducting mechanism, in which protons diffused by hopping along the cross-linking sites between the sulfonic groups of SG and the pyrrole rings of PBI, while electrons were transported *via* the highly electron conductive SG, as shown in Fig. 5. By adding SG, the membrane became more compact due to the smaller interlayer spacing and swelling ratio. The PBI–TGIC/SG membrane can separate H_2 from the H_2/CO_2 mixture (50 : 50 v/

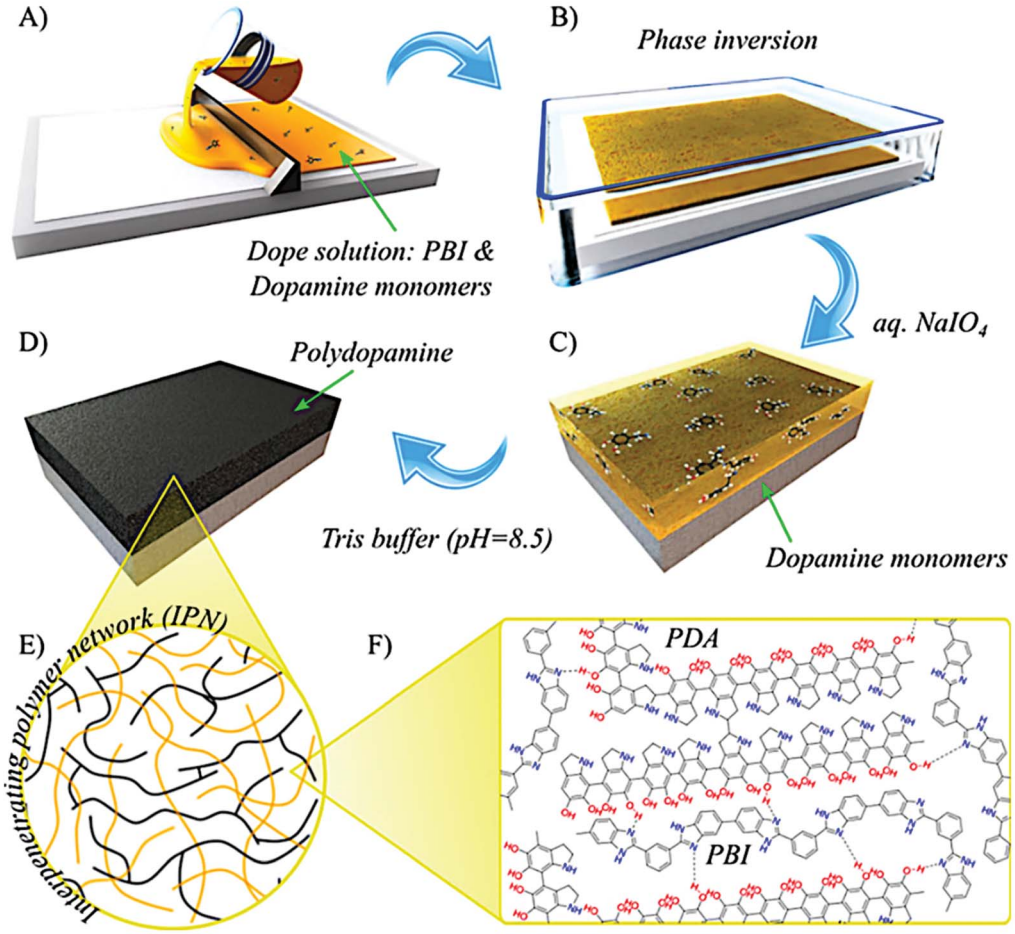

Fig. 4 Schematic overview of the membrane fabrication methodology for *in situ* polymerized polydopamine (PDA)/polybenzimidazole (PBI) interpenetrating polymer network (IPN): (A) casting a dope solution comprising PBI and dopamine monomers, (B) phase inversion in water, (C) immersing the membrane in an aqueous NaIO4 initiator, and (D) *in situ* polymerization of dopamine in a tris buffer solution. (E) IPN of linear PBI and branched PDA. (F) Molecular-level interactions between PBI and PDA polymers. Reproduced with permission from ref. 60, copyright 2019, ACS Publications.

v)) with 99.99% selectivity (infinite) and a high permeability of up to 1676 barrer at 300 °C due to the mixed conducting property of the composite membrane.

2.2 Changes of the main chain structure in PBIs

Although *m*-PBI has an industrially attractive H_2/CO_2 selectivity at elevated temperatures, its low H_2 permeability (about 1–2 barrer at 35 °C)[64,71,72] hinders its broad membrane applications for H_2 separation unless an ultrathin dense-selective layer can be fabricated. The low permeability can be attributed to its limited free volume that resulted from the effective chain packing owing to the strong H-bonding interactions and π–π stacking,[73–76] as elucidated in Fig. 6. Therefore, many attempts have been made to modify its mainchain structure that can improve the gas permeability while simultaneously maintaining its high H_2/CO_2 selectivity. Industrially, *m*-PBI is synthesized by a two-stage melt-solid polycondensation reaction which is more conducive for the large-scale production but usually produces the polymer with a low molecular weight owing to heterogeneous reaction conditions.[73] Moreover, PBIs made from the monomer of 3,3′-diaminobenzidine (DAB) (also referred to as 3,3′-4,4′ tetraaminodiphenyl) have very limited solubility in common polar aprotic solvents due to the rigid rod-like molecular structure and strong intermolecular H-bonding.[77] As a result, the commercially available *m*-PBI polymer, even with a low molecular weight (M_W) (*i.e.*, Celazole® S26 PBI with a M_W of 27 000 g mol^{-1} and an intrinsic viscosity of 0.70 dl g^{-1}), shows very poor solubility in common solvents, Therefore, it is often difficult to fabricate *m*-PBI into industrially applicable membranes.

Various molecular designs and modifications have been proposed to improve the gas permeability of PBIs including optimization of the main chain structure, N-substitution modification, as well as aforementioned chemical cross-linking modifications. It is well known that systematically alternating the backbone structure of a polymer with inhibited chain packing and mobility tends to increase permeability while maintaining or increasing selectivity.[78,79] Therefore, by introducing bulky groups into the PBI main chains, one can increase the distance between molecular chains and enlarge the free

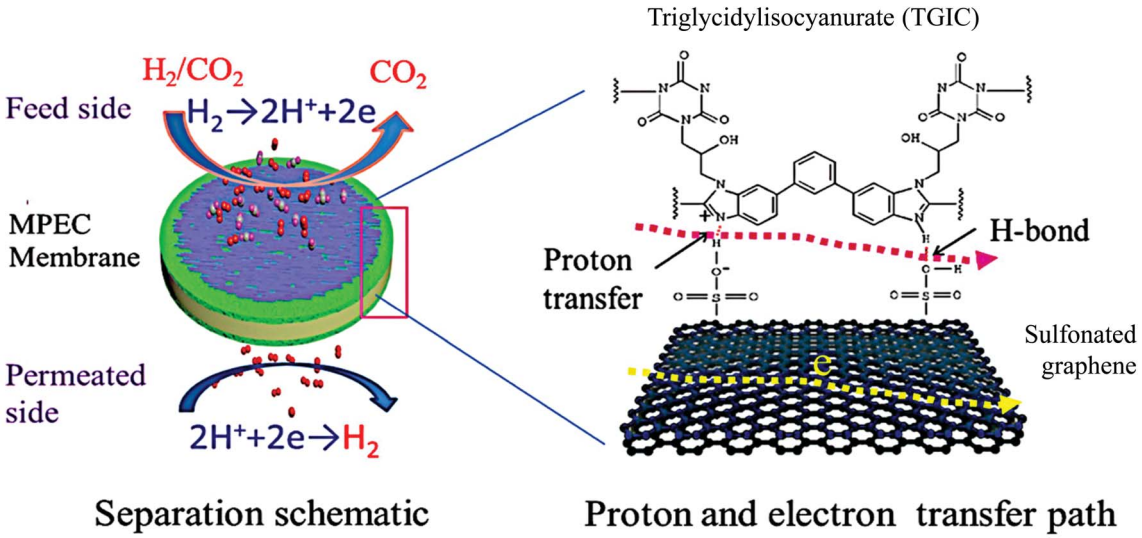

Fig. 5 Schematic diagram of the mixed conducting mechanism in the MPEC PBI-TGIC/SG membrane. Reproduced with permission from ref. 70, copyright 2021, the Royal Society of Chemistry.

volume without seriously losing the chain rigidity. As listed in Table 1, structurally modified PBI materials were obtained by varying the acid moiety during PBI syntheses *via* solution polymerization using either DAB or substituted aromatic dicarboxylic acids. The optimized PBI materials had a reduced chain packing density, but slightly decreased thermal stability.[73,74,80] In addition, the introduction of (1) *tert*-butyl groups in PBI–BuI and (2) hexafluoroisopropylidene groups in PBI–HFA improved solubility in pyridine and NMP, while the incorporation of bromine in PBI–BrT and PBI–DBrT enhanced their solvent solubility. However, the solubility of PBI-T was reduced due to the improvements of chain rigidity and symmetry, and intermolecular attraction. All the derived PBIs were amorphous in nature and exhibited high degradation temperatures (>400 °C).

As shown in Fig. 7, Li *et al.* synthesized four PBI derivatives containing bent and rigid configurations that possessed bulky side groups and could frustrate close chain packing.[73] Comparing with commercial *m*-PBI, the structurally modified PBIs had higher molecular weights, slightly decreased thermal stabilities, and enhanced organo-solubilities. Table 2 confirms that the introduction of bulky, flexible and frustrated functional groups into the PBI backbone effectively produced new PBIs with much higher H_2 permeability. However, these PBI derivatives showed a lower H_2/CO_2 selectivity range of 5–7 than that of *m*-PBI because of the trade-off relationship between gas permeability and selectivity. As shown in Fig. 8, all PBI-based membranes exhibit higher gas separation performance than the 2008 Robeson's upper bound prediction at 250 °C (ref. 65) and are promising materials for H_2 separation from syngas at high temperatures. Among these polymers, the 6F–PBI membrane had an interesting relationship between CO_2 permeability and temperature because its permeability remained nearly constant from near-ambient temperature to 250 °C.[73] This unique phenomenon resulted from the combined effects of temperature-dependent solubility and diffusivity. At low temperatures, there was a strong CO_2–polymer interaction due to the presence of highly electronegative 6F groups, while at high temperatures, CO_2 solubility decreased rapidly but diffusivity increased quickly. This led to an almost constant CO_2

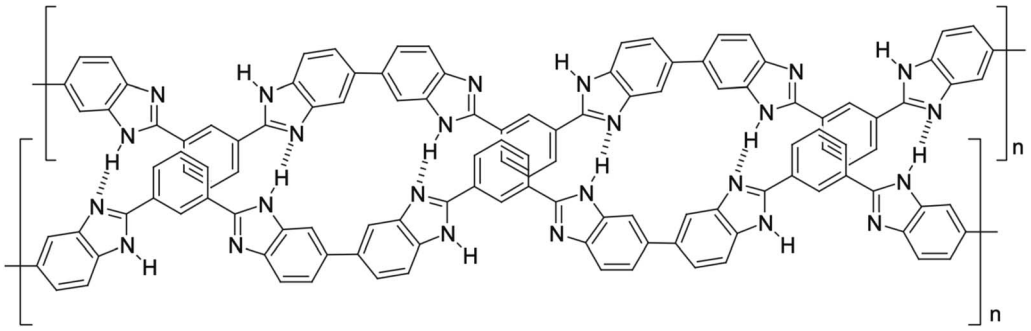

Fig. 6 Representation of PBI structural packing: π–π stacking and hydrogen bonding. Reproduced with permission from ref. 76, copyright 2016, Elsevier.

Table 1 Polybenzimidazoles based on 3,3′-diaminobenzidine (DAB)[a] or tetraaminodiphenylsulfone (TADPS)[b]

PBI polymer abbreviation	Dicarboxylic acid, HOOC–R–COOH	R Chemical structure	Polymerization solvent, T (°C)	IV (dL g^{-1})	Ref.
[a]PBI-I	Isophthalic acid (IPA)	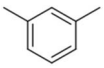	PPA[c], 200 °C	1.4	Kumbharkar *et al.* 2006,[74] 2009 (ref. 80)
[a]PBI-T	Terephthalic acid (TPA)		PPA[c], 200 °C	1.8	Kumbharkar *et al.* 2009 (ref. 80)
[a]PBI-Bul	5-*tert*-Butylisophthalic (Bul)	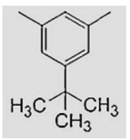	PPA[c], 200 °C	1.3	Kumbharkar *et al.* 2006,[74] 2009 (ref. 80)
[a]PBI-HFA	4,4′-(Hexafluoroisopropylidene)bis (benzoic acid) (HFA)	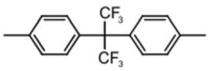	PPA[c], 200 °C	1.4	Kumbharkar *et al.* 2006,[74] 2009 (ref. 80)
[a]PBI-BRT	2-Bromoterephthalic acid (BrTPA)	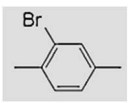	PPA[c], 200 °C	1.3	Kumbharkar *et al.* 2009 (ref. 80)
[a]PBI-DBRT	2,5-Dibromoterephthalic acid (DBrTPA)	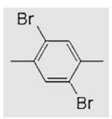	PPA[c], 200 °C	1.3	Kumbharkar *et al.* 2009 (ref. 80)
[a]PBI-2,6Py	2,6-Pyridinedicarboxylic acid (PyA)	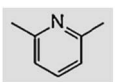	PPA[c], 200 °C	0.9	Kumbharkar *et al.* 2009 (ref. 80)
[a]6F-PBI	2,2-Bis(4-carboxyphenyl)-hexafluoropropane	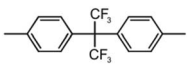	PPA[c], 220 °C	1.4	Li *et al.* 2014 (ref. 73)
[a]PBI-PFCB	4,4′-((1,2,3,3,4,4-Hexafluorocyclo-butane-1,2-diyl) bis(oxy))dibenzoic acid	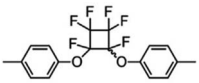	Eaton's reagent, 140 °C	0.73	Li *et al.* 2014 (ref. 73)
[a]PBI-BTBP	2,2′-Bis(trifluoromethyl)benzidine	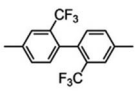	Eaton's reagent, 140 °C	1.6	Li *et al.* 2014 (ref. 73)
[a]PBI-phenylindane	1,1,3-Trimethyl-3-phenylindan-4′,5-dicarboxylic acid	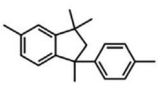	PPA, 195 °C	0.8	Li *et al.* 2014 (ref. 73)
[b]TADPS-OBA	4,4′-Oxybis(benzoic acid) (OBA)	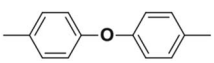	Eaton's reagent, 140 °C	—	Borjigin *et al.* 2015 (ref. 85) Stevens *et al.* 2020 (ref. 72)
[b]TADPS-TPA	Terephthalic acid (TPA)		Eaton's reagent, 140 °C	—	Borjigin *et al.* 2015 (ref. 85) Stevens *et al.* 2020 (ref. 72)
[b]TADPS-IPA	Isophthalic acid (IPA)	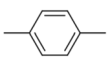	Eaton's reagent, 140 °C	—	Borjigin *et al.* 2015 (ref. 85) Stevens *et al.* 2020 (ref. 72)

[a] Polybenzimidazoles were synthesized by a solution polycondensation method based on 3,3′-diaminobenzidine (DAB) and dicarboxylic acid. [b] Polybenzimidazoles were synthesized by a solution polycondensation method based on tetraaminodiphenylsulfone (TADPS) and dicarboxylic acid. [c] PPA, polyphosphoric acid.

permeability over the evaluated temperature range. Owing to the high H_2 permeance and thermal resistance at elevated temperatures, 6F–PBI or PBI–HFA has been used to seal defects on the selective surface of PBI hollow fiber membranes to mitigate the influence of pin–hole defects,[81,82] similar to the role of commonly adopted silicone rubber. Since 6F–PBI has a high H_2 permeability due to the presence of highly disrupted and loosely packed hexafluoroisopropylidene diphenyl groups while *m*-PBI has a high H_2 selectivity owing to the tightly packed phenylene group, Singh *et al.* synthesized 6F–PBI/m-PBI copolymers with a tailorable permeability and selectivity, and a high inherent viscosity.[83]

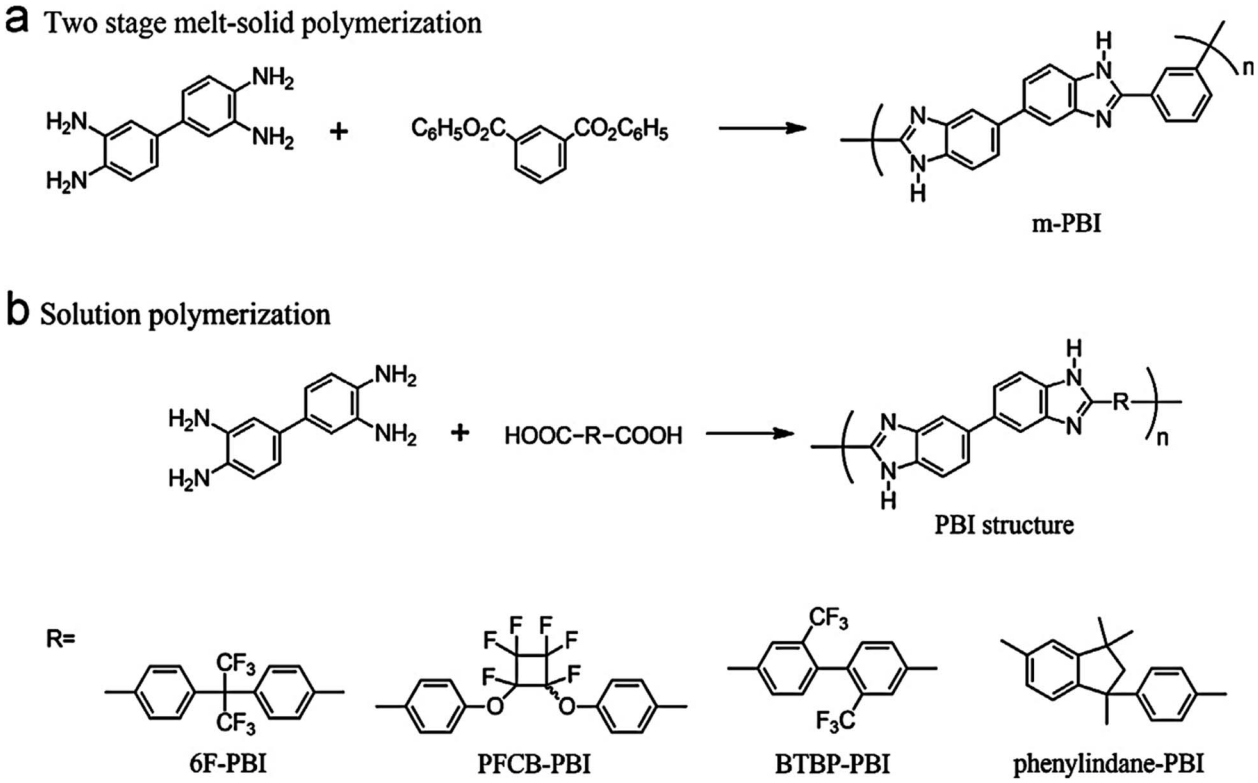

Fig. 7 Synthetic schemes of PBI derivatives (a. *m*-PBI; b. 6F-PBI, PFCB-PBI, BTBP-PBI, and phenylindane-PBI). Reproduced with permission from ref. 73, copyright 2014, Elsevier.

Table 2 Permeability and selectivity of the PBI derivative membranes[a]

PBI membrane	Feed gas	ΔP	T (°C)	H_2 permeance (GPU)	H_2 permeability (Barrer)	H_2/CO_2 selectivity	Ref.
PBI–I	Pure	2.1×10^6 Pa (300 psia)	35	—	0.63	3.8	Kumbharkar *et al.* 2006,[74]
PBI–T					0.16	—	2009 (ref. 80)
PBI–BuI					10.66	5.58	
PBI–HFA					12.15	4.18	
PBI–BrT					0.38	—	
PBI–DBrT					1.89	—	
PBI–2,6Py					1.38	—	
m-PBI	Pure	3.4×10^5 Pa (50 psia)	250	3.6	76.81	23.03	Li *et al.* 2014 (ref. 73)
6F-PBI				162.1	997.2	5.174	
BTBP-PBI				89.07	710.4	7.111	
Phenylindane-PBI				24.55	480.6	6.522	
PFCB-PBI				22.55	323.1	6.604	
TADPS-OBA	Pure	1.0×10^6 Pa (10.0 atm)	35	—	5.7 ± 0.2	10	Borjigin *et al.* 2015 (ref. 84)
TADPS-TPA					5.5 ± 0.3	20	
TADPS-IPA					3.6 ± 0.3	32	
m-PBI	Pure	3.0×10^5 Pa (3.0 atm)	190	—	22.1 ± 0.6	23.3 ± 0.9	Stevens *et al.* 2020 (ref. 72)
TADPS-OBA					38 ± 1	18 ± 2	
TADPS-TPA					31 ± 3	24.6 ± 0.9	
TADPS-IPA					30.1 ± 0.8	9.7 ± 0.4	
m-PBI[b]	Pure	1.4×10^5 Pa (20 psia)	43	—	4.0	16.8	Li *et al.* 2014 (ref. 73)
m-PBI[c]	Pure	1.1×10^6 Pa (11.0 atm)	35	—	2.0 ± 0.1	12 ± 1	Zhu *et al.* 2017 (ref. 64)
m-PBI	Pure	2.7×10^5 Pa (2000 torr)	35	—	1.11 ± 0.03	11.1 ± 1.1	Panapitiya *et al.* 2015 (ref. 71)
m-PBI	Pure	3.0×10^5 Pa (3.0 atm)	35	—	2.4 ± 0.1	24 ± 1	Stevens *et al.*2020 (ref. 72)

[a] 1 Barrer = 1×10^{-10} cm^3 (STP) cm cm^{-2} s^{-1} cmHg^{-1}, 1 GPU = 1×10^{-6} cm^3 (STP) cm^{-2} s^{-1} cmHg^{-1} = 7.50×10^{-12} m s^{-1} Pa^{-1}. [b] Estimated from their figures.[73] [c] The *m*-PBI membrane was fabricated from a Celarole® S10 PBI solution.

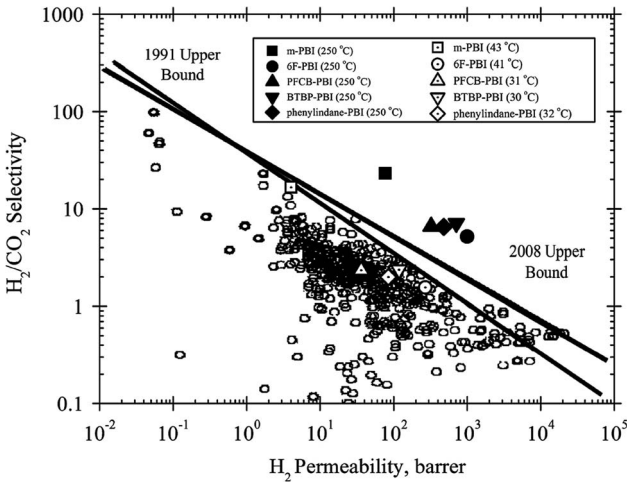

Fig. 8 Robeson plot comparing the PBI derivative membranes with other polymeric membranes tested for the H_2/CO_2 separation. Reproduced with permission from ref. 73, copyright 2014, Elsevier.

The H_2/CO_2 separation performance of these copolymers surpassed the 2008 Robeson's upper bound at 250 °C.[65]

Fig. 9 shows another type of highly permeable thermally rearranged PBI (TR-PBI) membranes with microporous characteristics (*i.e.*, high free volume fraction and large average *d*-space) by the scheme from polypyrrolone (PPL) *via* the ring-opening reaction in an alkaline solution, and a thermal treatment followed by decarboxylation at 450 °C.[84] The TR-PBI membranes treated at 450 °C had a H_2 permeability of 1779 barrer and an ideal H_2/CO_2 selectivity of 1.1 at 25 °C. Although the H_2/CO_2 selectivity was low, it could be improved by increasing the feed temperature since the CO_2 permeability would drop significantly due to the decrease in CO_2 solubility at higher temperatures of more than 200 °C.

Borjigin *et al.* synthesized PBIs containing sulfonyl groups and fabricated them as high temperature membranes for H_2/CO_2 separation.[85] As illustrated in Fig. 10, the rigid 3,3-diamine monomer was substituted by the monomer of 3,3′,4,4′-tetraaminodiphenylsulfone (TADPS). The flexible and kinked sulfonyl linkage in the main chain structure not only enhanced the PBI solubility but also inhibited the chain packing and interchain interactions.[72] As a result, these novel PBIs had enhanced T_g and solubilities in dipolar aprotic solvents that facilitated the solution casting of thin and defect-free membranes. Table 2 also summarizes their gas separation properties for H_2/CO_2 separation at 35 °C.

N-substituted polybenzimidazoles were also synthesized by using selective bulky or flexible side groups in order to break the intermolecular H-bonding, disrupt chain packing and increase the gas permeability.[86] Although both the T_g and degradation temperature of N-substituted PBIs became lower owing to the increase in chain flexibility, the gas permeability increased while the gas selectivity declined. Similarly, the gas sorption capability increased because of the loose chain packing and weak H-bonding. In addition, the solubility in solvents of chloroform and trichloroethylene was enhanced.[86] As a result, N-substituted PBIs have gas separation properties more suitable for other gas pairs rather than for H_2/CO_2 separation.[87]

As a class of porous organic frameworks (POFs), benzimidazole-linked polymers (BILPs) have been synthesized by the condensation reaction between aryl-*o*-diamines and aldehydes in DMF to form amorphous powders with network structures.[88,89] The resultant BILPs were insoluble in solvents and had outstanding thermal and chemical stabilities, as well as high CO_2 uptakes. They may be a good candidate for CO_2 capture, storage as well as other industrial separations. Shan *et al.* prepared defect-free BILP membranes by using the interfacial polymerization method and the resultant membrane exhibited excellent separation performance with a permeance of 24 GPU and H_2/CO_2 selectivity of 40 at 150 °C using an equimolar H_2/CO_2 mixture as the feed at 1 bar.[90] Wang *et al.* followed the same approach and synthesized BILP membranes suitable for He/CH_4 separation.[91] Both membranes have separation performance surpassing the 2008 Robeson upper bounds. So far, BILP-based PBI membranes have not received much attention especially on the fabrication and applications of their HFMs.

3. Fabrication of PBI hollow fiber membranes (HFMs)

Polymeric membranes are generally fabricated by the phase inversion process where a homogeneous polymer solution consisting of solvents as the continuous phase converts into a three-dimensional polymeric network where the dissolved polymers become the continuous phase. The phase inversion can be induced by solvent evaporation (*i.e.*, the dry-cast), non-solvent/solvent exchange (*i.e.*, the wet-cast), non-solvent absorption, and cooling (*i.e.*, the thermal-cast).[92]

3.1 Fundamental of asymmetric HFM formation by non-solvent induced phase separation

During the non-solvent induced phase separation (NIPS), the phase separation of a polymer solution is induced by composition changes due to the inflow of non-solvents and the outflow of solvents. The change in composition induces the phase separation of the dope solution and leads to the formation of the membrane matrix. Membranes prepared *via* the NIPS method would have an asymmetric structure with different degrees of porosity across the membrane thickness. Since the dense skin layer and the porous substrate layer are made of the same material, it is referred to as integrally skinned asymmetric (ISA) membranes.

The NIPS process can be qualitatively illustrated by a triangle phase diagram which describes the thermodynamic interactions among the polymer, solvents, and non-solvents. The binodal curve divides the triangle into two regions, namely, a single-phase region where all components are miscible and a two-phase region where the homogeneous solution separates into a polymer rich phase and a polymer lean phase,[93,94] as shown in Fig. 11. During the phase inversion, the nascent membrane starts to cross the binodal curve, its composition is

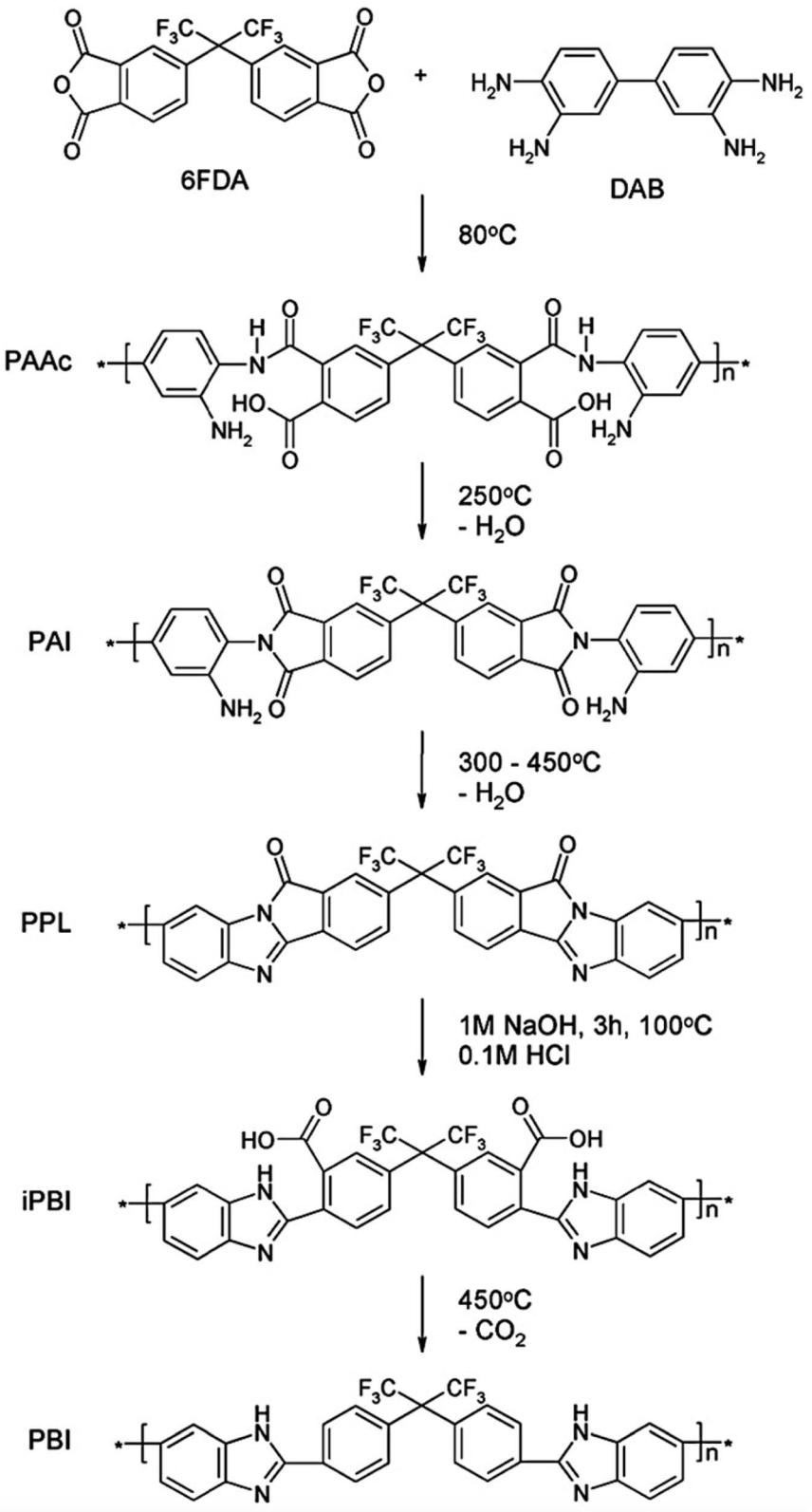

Fig. 9 Synthesis route to microporous polybenzimidazole (TR-PBI) from polypyrrolone (PPL) using a thermal rearrangement concept. Reproduced with permission from ref. 84, copyright 2010, Elsevier.

divided into two phases connected by a tie line. The polymer-rich and polymer-lean phases would eventually develop into the polymer matrix and pores, respectively. Ideally, the final morphology of as-cast flat-sheet membranes is mainly related to the initial casting composition, binodal curve position, and precipitation path if no external forces or factors are applied.

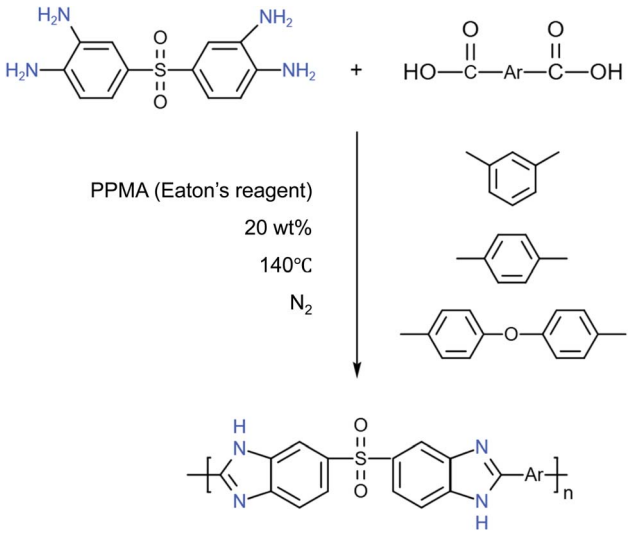

Fig. 10 Synthesis of polybenzimidazole using Eaton's reagent as a solvent.[72] PPMA (Eaton's reagent): phosphorus pentoxide/methanesulfonic acid.

Generally, kinetics will affect the precipitation path for a given polymeric solution, whereas thermodynamics controls the position of binodal points during the phase inversion.[93–96]

During the spinning of a hollow fiber membrane (HFM), a polymer solution and a bore fluid are extruded through a spinneret simultaneously and a nascent hollow fiber begins to form and then enters the coagulation bath where solvents and nonsolvents are fully exchanged, as shown in Fig. 12. The bore fluid that occupies the lumen space can be simply removed during the solvent exchange and drying steps. Different from flat-sheet membranes, the fabrication of hollow fibers involves two coagulants (*i.e.*, internal and external coagulants) which influences the formation of the inner and outer surfaces, respectively. Depending on the two coagulants' chemistry, solubility parameters and other factors, they may determine where the selective layer is formed. For example, the evaporation of volatile components in the air gap region can cause the outermost surface of the nascent hollow fiber to approach a vitrified state, thus a dense skin is formed on the outer layer of the hollow fiber. Once the nascent hollow fiber enters the coagulant bath, both inner and outer coagulants would diffuse into the hollow fiber and induce a porous substrate that provides the overall mechanical strength. In this way, a desirable integrally skinned asymmetric hollow fiber membrane with a dense layer on top of a porous substructure is formed. Spinning parameters have important influences on the phase inversion process, including dope and bore fluid compositions, dope viscosity, air gap distance, extrusion rates of the dope and bore fluid, and take-up speed. The manufacturing process of HFMs in large scale production is shown in Fig. 13.

Hollow fiber membrane modules have several advantages over both tubular modules and spiral-wound modules made of flat-sheet membranes, including a higher ratio of surface to volume and a much smaller footprint.[35,97,98] In addition, spiral wound modules require (1) a higher energy input due to the pressure drop along the spacer-filled channels and (2) extensive pre-treatment of feed solutions to reduce fouling.[99] In contrast, HFMs need less pre-treatment and operation maintenance while keeping a relatively high packing density. Due to the advances in multi-filament spinning capability, modern HFM fabrication systems have achieved exceedingly high productivity.[100] They can offer module surface area-to-volume ratios approaching 1000–10 000 m^2 m^{-3}.[35,101,102] Usually, a thick dense-selective layer in hollow fiber membranes may offset some of the surface area advantage of the fiber configuration, but it is feasible to increase the module productivity (*i.e.*, surface area) per unit volume by an order of magnitude.[33] In

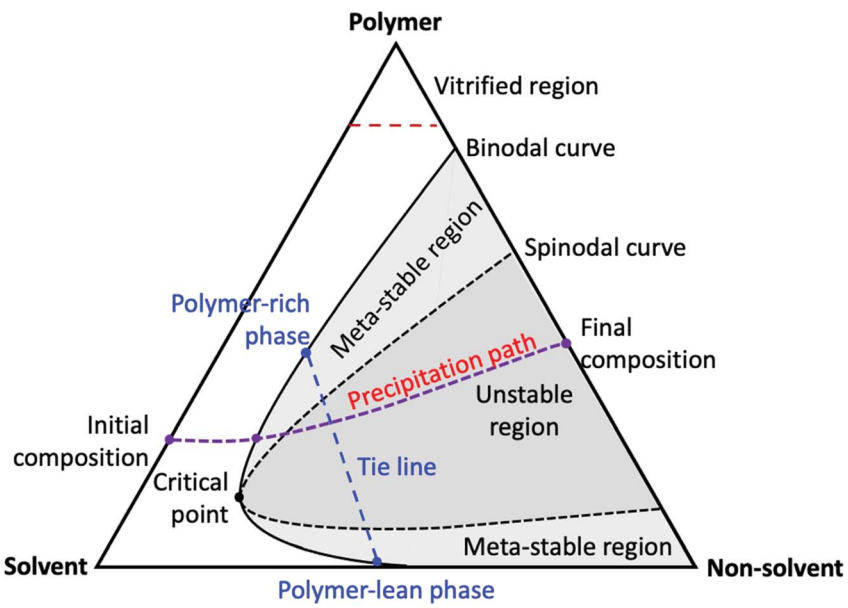

Fig. 11 Schematic of the ternary phase diagram of a polymer–solvent–nonsolvent system.

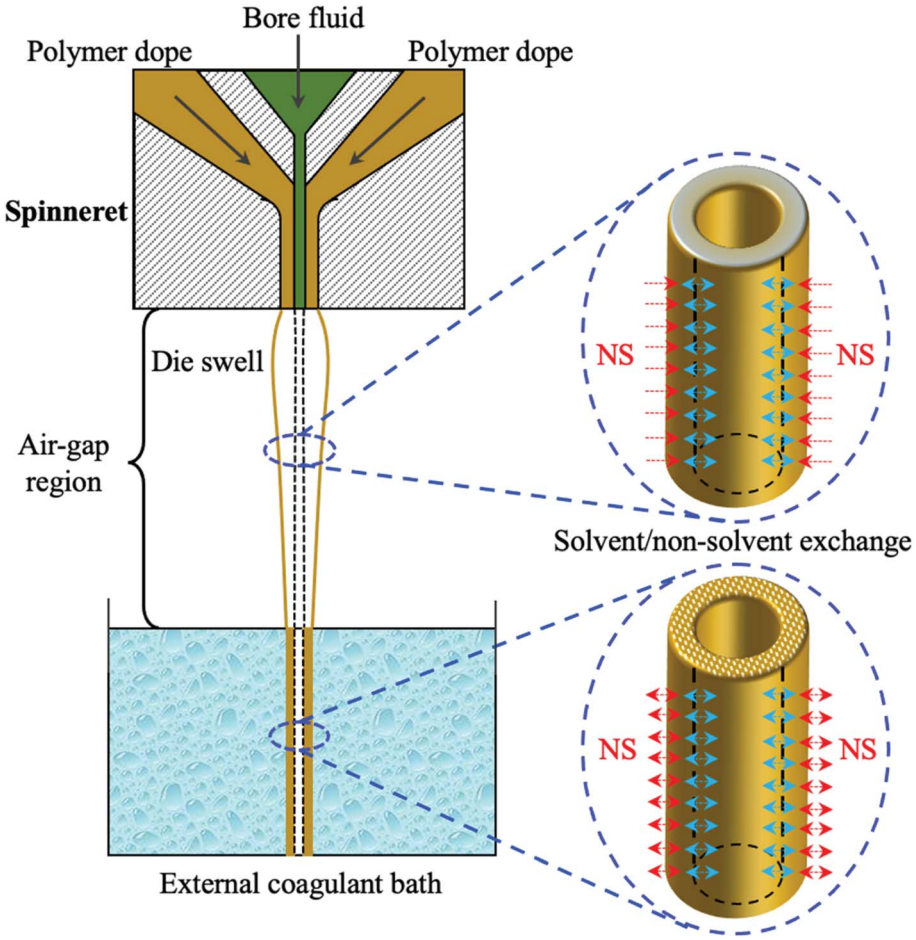

Fig. 12 Schematic of the enlarged regions inside and outside of the spinneret and the formation of a nascent hollow fiber membrane *via* a NIPS process.

addition, HFMs can withstand a high transmembrane pressure difference (up to 70 bar) while the manufacturing cost is 5–20 times lower than those of equivalent membranes used for spiral wound modules in large-scale gas separation applications.[97]

3.2 State-of-the-art technologies to design integrated skinned PBI HFMs

The unique macromolecular characteristics of PBI make it a highly challenging polymer to develop integrally skinned asymmetric membranes with a controllable morphology. The rigid rod-like molecular structure produces strong H-bonding and π–π stacking between PBI molecular chains,[73–76] which not only limits its dissolution in common organic solvents but also often results in brittle membranes. PBI is only soluble in high boiling point aprotic solvents including DMAc, NMP, and DMF owing to their nitrogen functionality. Accordingly, commercially available highly concentrated PBI solutions are prepared at a high temperature up to 240 °C under high pressures.[103] LiCl is commonly added into the PBI/DMAc solution during dissolution to improve polymer solubility and maintain solution stability.[104,105]

3.2.1 The formation of macrovoids during NIPS. Fabricating PBI HFMs using a DMAc/water or NMP/water mixture as the bore fluid and water as an external coagulant has been reported for gas[81] and PV[106] applications. The resultant HFMs had either a layer of large macrovoids or two layers of small macrovoids located at the inner and outer surface regions. When using DMAc/EG or DMAc/EG/THF as the bore fluid, the macrovoids near the inner layer were eliminated.[42,107] However, these PBI HFMs with half-part macrovoids were still very brittle and might collapse after drying. This drawback has created a tremendous challenge to fabricate PBI into self-supported membranes and modules. To overcome the inherent difficulty of forming a desirable HFM and minimize the structure collapse during the drying, one must understand the fundamentals of hollow fiber spinning and control the final membrane morphology by optimizing the spinning conditions.

It is well known that macrovoids may be formed in polymeric membranes *via* NIPS if the nonsolvent/solvent exchange is very rapid while the rapid solvent exchange is necessary to create an ultrathin dense-selective skin on the membrane surface. In general, macrovoids with finger-like and tear-drop shapes in asymmetric HFMs are considered as weak mechanical points

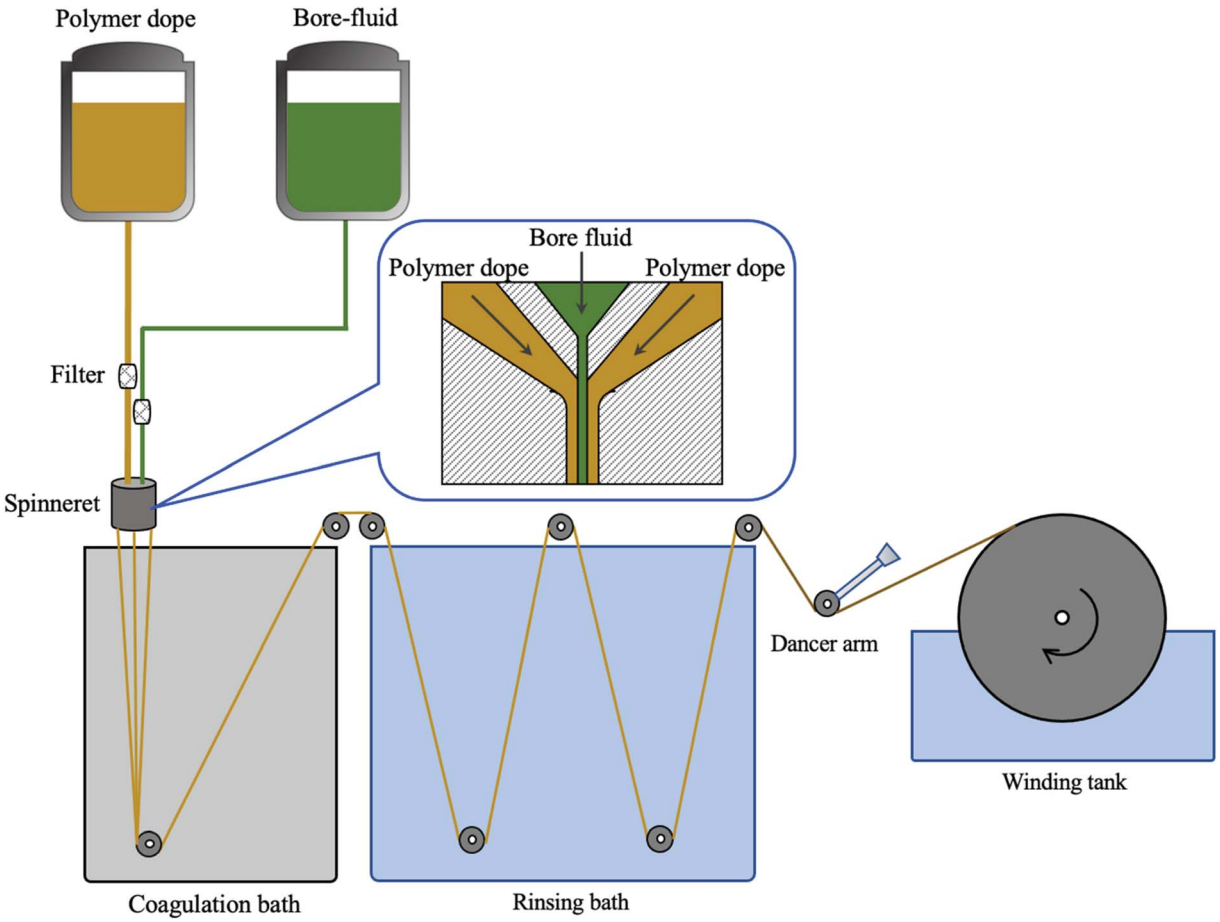

Fig. 13 The manufacturing process of hollow fiber membranes in large-scale production.

which generate high stress areas and cause fiber failure under vibrations in membrane bioreactors (MBRs) or high pressures for gas separation especially at high temperatures.[35,95,96,108] When the operation temperature is close to the T_g of the polymer, the enhanced chain mobility leads to increasing the susceptibility of structural collapse at these defect locations under high transmembrane pressures.[109] In addition, the presence of macrovoids near the outer surface of HFMs often results in a defective selective layer.[82] The technology to develop macrovoid-free HFMs is crucial for the rapidly growing membrane applications.

The origin of macrovoids is one of the debatable subjects among membrane scientists in the last 5 decades. Early researchers believed it could arise from instantaneous liquid–liquid demixing and the nucleation of droplets in the lean polymer phase due to the diffusion-driven mechanism,[110–112] while others thought it could start from local mechanical instability, surface rupture and non-solvent intrusion, followed by rapid nucleation of droplets in the lean polymer phase.[113,114] Other mechanisms such as Marangoni effects,[115] osmosis pressure[116] and solutocapillary convection mechanism[117–119] had also been proposed. The solutocapillary convection mechanism consisted of diffusion and Marangoni force generated by local surface tension gradients. Clearly, macrovoid formation may involve multiple mechanisms taking effect simultaneously due to the existence of large differences in viscosity and concentration gradients between the two phases.[35,96] Today, two mechanisms as well as their combined mechanism are mostly accepted for macrovoid formation: (1) the diffusion mechanism with the aid of solutocapillary convection, and (2) local surface instability, skin rupture and non-solvent intrusion.

Several methods have been proposed to suppress macrovoid formation, such as: (1) increasing polymer concentrations or dope viscosity[120] or adding components with high viscosity,[121,122] (2) inducing delayed demixing or gelation,[116,123] (3) adding surfactants in dopes,[124] (4) decreasing dope temperature[125] or increasing temperature in the coagulation bath,[126] (5) spinning at high shear rates or high elongational rates.[120,127,128] Although increasing the dope viscosity by the aforementioned methods is an effective means to lower non-solvent intrusion and minimize macrovoid formation, it often leads to a thick dense-selective layer.[96,129] One must also choose a suitable solvent–nonsolvent system during the phase inversion process to produce membranes with the desirable morphology, mechanical properties and separation performance.

Solubility parameter has been extensively used to predict the solubility of polymers in solvents. The Hanson solubility parameter (δ) of a material is determined by the group

contributions from its structural elements based on dispersion forces (referred to as δ_d), polar interactions (δ_p) and hydrogen bonding (δ_h).[130] The total solubility parameter (δ_T) of a polymer is a sum of these three contributions, as written in eqn (1). When dissolving a polymer in a solvent, the difference in their solubility parameters, $\Delta\delta_{S-P}$, can be calculated from eqn (2). The combined parameter, δ_v, is defined as eqn (3).[131]

$$\delta_T = (\delta_d^2 + \delta_p^2 + \delta_h^2)^{1/2} \quad (1)$$

$$\Delta\delta_{S-P} = [(\delta_{d,S} - \delta_{d,P})^2 + (\delta_{p,S} - \delta_{p,P})^2 + (\delta_{h,S} - \delta_{h,P})^2]^{1/2} \quad (2)$$

$$\delta_v = (\delta_d^2 + \delta_p^2)^{1/2} \quad (3)$$

Table 3 lists the solubility parameters of PBI, some solvents and non-solvents. For a given polymer, one can determine the "solubility circle" associated with the polymer and solvents according to the $\Delta\delta_{S-P}$ values. When the $\Delta\delta_{S-P}$ value is less than 5, the solvents inside this circle are considered as "good" solvents that will dissolve or swell the polymer.[132] Usually, the combined parameter δ_v is plotted against δ_h to compare various polymer/solvent systems. As illustrated in Fig. 14, DMAc, NMP and acetone, are good solvents for PBI although PBI is insoluble in acetone, while MeCN, ethylene glycol, and THF are non-solvents (NS).

The solubility parameter difference between the solvent and non-solvent will influence the solvent exchange rate and alter the polymer solubility in the transient polymer/solvent/non-solvent mixture during the non-equilibrium state of the phase inversion process. Generally, a closer solubility parameter between the polymer solution and nonsolvent would result in a delayed demixing, thereby obtaining a more porous membrane structure without macrovoids. In contrast, if they have a larger difference in solubility parameter, it may result in an asymmetric membrane with a dense nonporous top layer with macrovoids due to the instantaneous dimixing.

3.2.2 State-of-the-art technologies to design macrovoid-free PBI HFMs. Dahe *et al.* systematically investigated the fundamentals of wet spinning asymmetric PBI HFMs consisting of a porous support structure and dense-selective layers.[132] They found that a dope containing 21.3 wt% PBI in DMAc had a sufficient viscosity that could prevent macrovoid formation in PBI HFMs. In addition, the formation of macrovoids in wet-spun PBI membranes was dependent on the ratio of

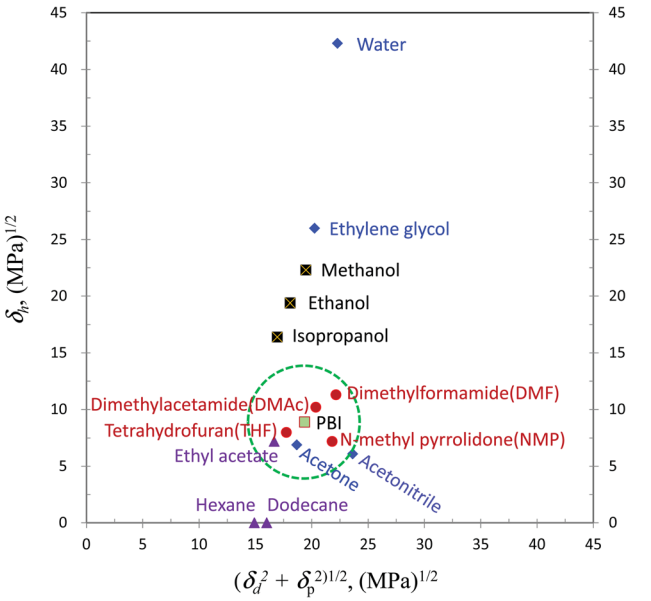

Fig. 14 Solubility parameter plot for PBI and organic solvents. δ_d, δ_p, and δ_h (Hansen parameters) are the contribution of dispersive force, polar force and hydrogen bonding, respectively. The green circle represents a solubility parameter difference between PBI and organic solvent of less than 5.[82]

nonsolvent inflow to solvent outflow. When using acetone, methanol and ethanol as bore fluids, because acetone has (1) the smallest diffusivity in DMAc among these three solvents and (2) a close solubility parameter with the PBI/DMAc dope, the inflow of acetone to the nascent hollow fiber was mild and slightly larger than the outflow of DMAc, thus resulting in a porous substrate. In contrast, methanol has the highest diffusivity in DMAc, it induced a rapid nonsolvent/solvent exchange and resulted in PBI membranes with many large macrovoids near the inner layer. Usually, a dense-selective layer is formed when its solvent outflow is faster than the nonsolvent inflow. An acetone solution containing 1–2 wt% water was employed as the external coagulant because acetone had a small diffusivity in DMAc and the presence of 1–2 wt% water in acetone could facilitate the outflow of DMAc. In addition, the inflow of water into the nascent hollow fiber would be slower than the outflow of DMAc due to the high dope viscosity. The

Table 3 Solubility parameters of PBI, solvents and non-solvents[130]

Polymer or Solvent	δ_p (MPa$^{1/2}$)	δ_d (MPa$^{1/2}$)	δ_h (MPa$^{1/2}$)	δ_P or δ_S (MPa$^{1/2}$)	$\delta_{S\text{-}P}$ (MPa$^{1/2}$)
PBI	8.7	17.3	8.9	21.3	—
DMAc	11.5	16.8	10.2	22.8	3.1
NMP	12.3	18.0	7.2	23.0	4.0
DMF	13.7	17.4	11.3	24.9	5.5
THF	16.8	5.7	8.0	19.4	14.2
MeCN	18.0	15.3	6.1	24.4	9.9
Acetone	10.4	15.5	6.9	20.0	3.2
Toluene	18.0	1.4	2.0	18.2	19.7
EG	17.0	11.0	26.0	32.4	20.0
Water	16.0	15.5	42.3	47.8	34.2

resultant defect-free PBI HFMs had a H_2 permeance ranging from 7 to 21 GPU while the H_2/CO_2 selectivity varying from 22.4 to 14 at 250 °C.

A breakthrough was made by Singh *et al.* who added acetonitrile in diluted PBI solutions, discovered its effectiveness to augment the dope viscosity and produced dry-jet wet-spun PBI HFMs with a desirable morphology; namely, an outer dense-selective layer and a macrovoid-free porous substrate.[82] Acetonitrile (MeCN) was chosen because it (1) is a weak solvent to PBI, (2) is a low boiling solvent (82 °C), (3) is highly soluble in water, and (4) has smaller MW than DMAc (41.05 *vs.* 87.12 g mol^{-1}). As a result, it increased the PBI dope viscosity due to the enhanced inter- and intra-molecular frictions among PBI chains and thus minimized the non-solvent intrusion during phase inversion, while its characteristics of high solubility in water, small MW and size, and low boiling point facilitated (1) the solvent/nonsolvent exchange in a wet-spinning process or (2) the solvent evaporation in a dry-jet wet-spinning process, thus forming a thin outer-selective layer. In addition, the authors adopted a PBI/DMAc/MeCN spinning solution very near to the precipitation point. Therefore, a small variation of dope composition due to the solvent/nonsolvent exchange could result in a uniform precipitation across the membrane. The obtained PBI HFMs have a bi-continuous sponge-like substructure that not only improved the overall mechanical strength of HFMs but also minimized the gas transport resistance. By manipulating the PBI HFM spinning parameters, the thickness of the dense-selective layer could be finely tuned between 200 and 2000 nm. The resultant PBI HFMs coated with 6F-PBI (*i.e.*, as a defect sealant) had a H_2 permeance one to two orders of magnitude higher than those reported by Kumbharkar *et al.*[81] and Dahe *et al.*[132] with a comparable H_2/CO_2 selectivity.

3.3 Dual-layer PBI HFMs

Henne *et al.* invented the co-extrusion technique to fabricate dual-layer asymmetric composite HFMs for hemodialysis in the late 1970s.[133] The formation mechanism and controlling parameters for dual-layer hollow fiber fabrication are complicated because two polymer solutions undergo phase inversion with different chemistries and rheological properties simultaneously.[134] However, the dual-layer co-extrusion technique offers many advantages over the single-layer one. For example, one can fully explore the use of expensive and high-performance polymers as the selective-layer material and reduce the transport resistance in the support layer by using another low-cost but mechanically strong material or a less concentrated polymer solution as the inner-layer dope. Compared to the membranes made by the layer-by-layer assembly, dip coating, and interfacial polymerization, the dual-layer co-extrusion technique has a higher productivity and more flexibility to tailor the HFM morphology.[35,96] Therefore, the co-extrusion technique has been extended to produce dual-layer HFMs for gas separation,[135–137] water nanofiltration,[138–140] pervaporation[141–144] and OSN.[145–147] Fig. 15 shows a typical dual-layer spinneret structure with triple orifices.

The most important issues with dual-layer HFMs are (1) delamination and (2) poor adhesion between the two polymeric layers. Delamination is often observed between the two layers due to their different shrinkage rates during phase inversion.[134] To overcome it, in addition to adjusting the spinning conditions, one can incorporate nanoparticles into the inner layer to lower its shrinkage rate or use an indented dual-layer spinneret to premix and enhance molecular diffusion between the two layers.[136] To improve the interfacial adhesion, the miscibility of the two polymers must be considered. A good adhesion can be achieved if the two polymers are partially miscible.[144] In addition, the incorporation of a small number of nanoparticles into the selective layer appears to be effective to achieve a good interfacial adhesion between the two layers.[139,148] One of the reasons arises from the fact that the addition of nanoparticles into the selective-layer dope may increase its viscosity, retard nonsolvent intrusion and mitigate the formation of large voids (*i.e.*, weak points) between the two layers.

A seamless interface is essential for the long-term structural integrity and separation performance of HFMs, especially at high pressures. PBI as the selective layer has been made into dual-layer HFMs through the co-extrusion process with other polymers. Delamination-free PBI/PAN (*i.e.*, PBI/polyacrylonitrile) dual-layer HFMs,[139] PBI/P84 (*i.e.*, PBI/co-polyimide, BTDA-TDI/MDI),[141,142,145] PBI/PEI (*i.e.*, PBI/polyetherimide),[106,149,150] and PBI/PES (*i.e.*, PBI/polyethersulfone)[151,152] have been fabricated and used for various membrane separations.

3.4 Blended PBI HFMs

To improve the permeability of PBI-based membranes, efforts have also been devoted to (1) blending PBI with a more permeable polyimide, and (2) incorporating functional nanoparticles to the PBI membrane matrix. Polyimides with a high FFV have been extensively studied for gas separation due to their superior separation performance[67,153] while the major deficiency of polyimides is their poor anti-plasticization property even under a low CO_2 pressure.[154] The miscibility and interaction between PBI and polyimides arise from the strong H-bonding between the N–H groups of PBI and the C=O groups of polyimides, thus some PBI/polyimide blends could display good miscibility over the entire composition range.[155,156] Since the incorporation of PBI into a polyimide matrix results in a higher chain packing density and a lower segmental mobility, this could lead to a higher diffusivity selectivity. In addition, the good processability of polyimides can compensate for the poor processability of PBI. HFMs made of PBI/Matrimid and PBI/PEI blends have been fabricated for gas separation,[67,157] pervaporation,[106,149,150,158] and oil–water treatment.[159]

3.5 Mixed matrix PBI composite HFMs

Mixed matrix membranes (MMMs) are designed by combining the strengths of the polymer matrix and functional nanofillers to surpass the upper performance limit of polymeric membranes.[160,161] Usually, the polymer matrix offers good processability, while the nanofillers provide high flux and

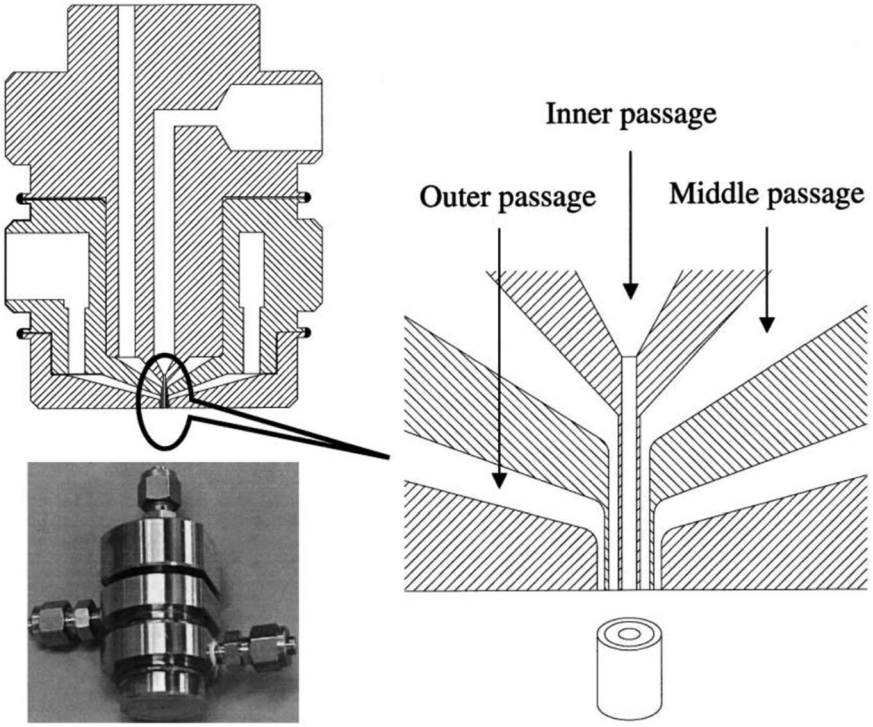

Fig. 15 Schematic diagram of spinneret for dual-layer hollow fiber spinning. Reproduced with permission from ref. 134, copyright 2002, Elsevier.

selectivity. The major challenge in fabricating high-performance PBI-based MMMs is how to uniformly disperse nanoparticles in the polymer matrix *via* adjusting the size and surface chemistry of nanoparticles and optimizing fabrication protocols.[160–164] PBI/carbon nanotubes, PBI/graphene, and PBI/graphene oxide, PBI/ZIF nanocomposites have motivated extensive research in the fields of supercapacitors, gas separation, strengthened materials, and fuel cells.[12] Since zeolitic imidazolate frameworks (ZIFs), a subfamily of metal–organic frameworks (MOFs), have characteristics of tailorable cavity sizes, high porosity and good affinity with polymers, exceptional thermal stability and outstanding chemical resistance,[161,165] high-performance PBI/ZIF MMMs have been molecularly designed to improve the H_2 separation performance at high temperatures.[166–168] As another key challenge to develop highly selective MMMs, the lack of interfacial adhesion may cause nanosized nonselective gaps between the fillers and PBI matrix which are detrimental to the filtration performance. By means of covalently grafting nanoparticles' surface with PDA or poly(*N*-isopropylacrylamide) (PNIPAM), they can become entangled with the membranes' polymer matrix to eliminate the undesirable gaps.[169,170]

4. Applications of PBI HFMs

Since the early 1970s, owing to their remarkable chemical resistance, mechanical strength and thermal stability, PBI HFMs have been widely explored in many membrane separations such as microfiltration (MF) and ultrafiltration (UF), reverse osmosis (RO), nanofiltration (NF), forward osmosis (FO), organic solvent nanofiltration (OSN), pervaporation (PV) and gas separation, particularly in aggressive environments. Here, we mainly summarize the historical background, market demands, major technology milestones and breakthroughs in the fabrication of PBI HFMs in the fields of RO, NF and OSN, PV and gas separations.

4.1 PBI HFMs for reverse osmosis (RO)

Due to its unique intermolecular hydrogen bonding, PBI was found to absorb up to 15% moisture that was equal to or higher than natural materials.[103] This early finding suggested PBI as an ideal hydrophilic material for RO and NF membranes because it also possesses the required thermal, physical and chemical stability over a wide range of pH. Therefore, asymmetric PBI RO flat sheets and HFMs were fabricated from PBI/DMAc/LiCl solutions by the dry-jet wet-spinning technology in the 1960s and 1970s.[103,171,172] Briefly, a PBI dope was metered and extruded through a multichannel spinneret, and an inert hydrocarbon liquid (such as dodecane) was delivered as the bore fluid through the lumen of the spinneret.[173] The obtained PBI membranes were post-treated and thermally annealed in a hot ethylene glycol solution at 140–180 °C to gain the permselectivity. A selective layer was formed on the outer surface while the fiber wall consisted of many finger-like macrovoids because water was used as the external coagulant.[171,174] Compared to cellulose acetate (CA) membranes, the 1st generation PBI RO membranes could withstand intensive chemical cleaning and was suitable for long-term use due to the unique properties of PBI in high-temperature and harsh environments.[171,175,176] Table 4 shows a comparison of RO performance between PBI and CA membranes at ambient and

elevated temperatures.[171] At ambient temperature they have comparable RO performance while PBI HFMs have superior RO performance to CA at elevated temperatures. Therefore, the early developed PBI RO HFMs were used in two specific applications; namely, seawater desalination in harsh environments and the recovery of washing water from space vehicles at pasteurization temperatures.[177]

Recently, both Wang *et al.*[178] and Wales *et al.*[179] fabricated PBI RO HFMs without finger-like macrovoids from PBI/DMAc/PVP/IPA dopes using MeOH/IPA mixtures as the internal and external coagulants. Fig. 16 shows one of their morphologies.[178] The PBI hollow fiber membranes exhibited good separation performance with a pure water permeability of 0.07 L m^{-2} h^{-1} bar^{-1} and a NaCl rejection of 99.0% after being treated with a 1000 ppm NaClO solution for 1 h. These performances were comparable to the commercial CTA RO HFMs produced by Toyobo Co. Ltd.[178] The PBI HFM demonstrated the stable operation of a single-stage RO system for treating concentrated flue gas desulfurization (FGD) wastewater with a salt rejection of 97%.[179] However, since polyamide-based thin-film composite (TFC) membranes invented in the 1980s[180,181] *via in situ* interfacial polymerization have impressively high RO performance and currently dominate the market of seawater desalination, the importance of PBI RO membranes has been significantly reduced.

4.2 PBI nanofiltration (NF) HFMs for water treatment

As a pressure-driven process, NF utilizes membranes to selectively remove multivalent cations and anions as well as larger size dissolved solutes while having limited rejections to monovalent ions.[182,183] The selective layer of NF membranes usually has a nominal MWCO varying from 200 to 1000 Da and a pore size of around 0.5–2.0 nm in diameter.[181–185] Separation mechanisms of NF membranes involve (1) size exclusion (*i.e.*, the steric effect) and (2) Donnan exclusion (*i.e.*, the partitioning interaction between

Table 4 Comparative performances of PBI and CA reverse osmosis membranes[171]

Operating temp. (°C)	Testing time (hr)	Final flux of CA membranes L m^{-1} h^{-1} (gal ft^{-2} d^{-1})	Final flux of PBI membranes L m^{-1} h^{-1} (gal ft^{-2} d^{-1})
70	5	20.4(12)	27.2(16)
120	5	34(20)	28.9(17)
167	20	8.5(5)	32.3(19)
194	5	0(0)	42.5(25)

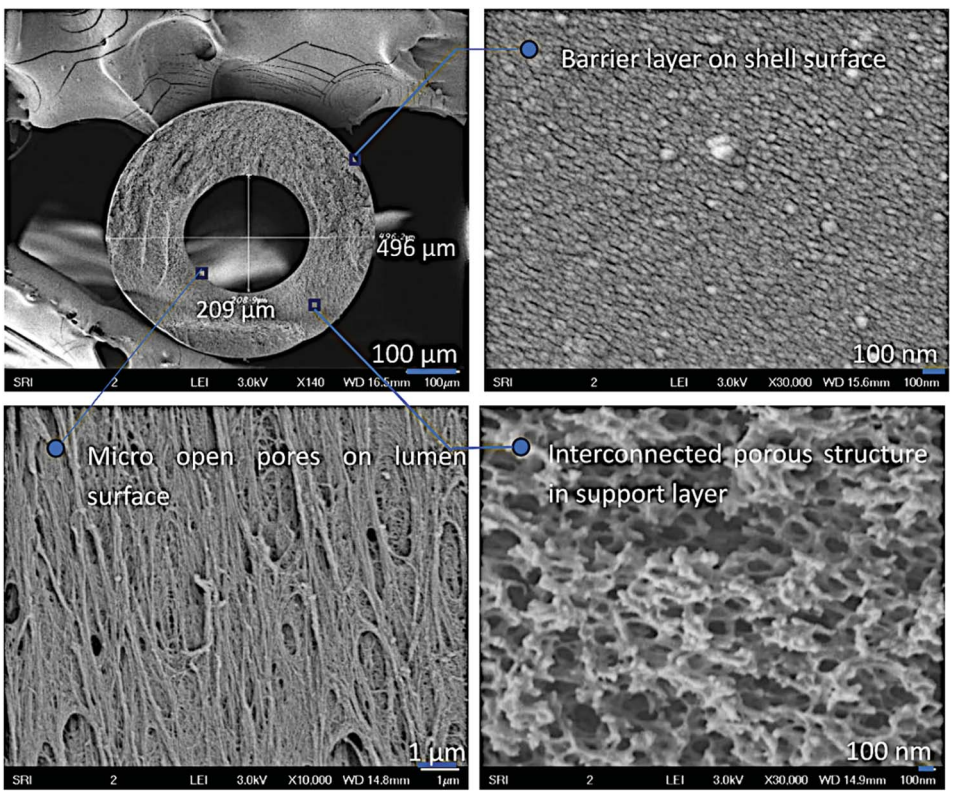

Fig. 16 Typical morphology of a polybenzimidazole RO hollow fiber membrane.Reproduced with permission from ref. 178, copyright 2018, MDPI.

the membrane and the feed solution).[186,187] Compared to RO, NF membranes have a relatively higher water permeability and a lower operation pressure, thus the latter consumes significantly less energy than the former. NF membranes have been broadly applied for water softening, removal of heavy metals from wastewater, treatment of municipal and industrial effluents, purification and concentration of biomedical products, and separating SO_4^{2-} from high salinity brines in the chlor-alkali process.[182–184] NF membranes can be made in various geometries (*i.e.*, flat sheet, hollow fiber and tubular) and packed into modules of different configurations for industrial applications. Compared to flat-sheet and tubular membranes, the hollow fiber geometry not only provides an extremely favourable surface area-to-volume ratio, but also greatly simplifies the hardware necessary for module fabrication. The desirable NF membranes for liquid separation must have the necessary chemical stability and robust mechanical strength to withstand high trans-membrane pressures employed during operations. Although flat-sheet NF membranes made by the TFC approach are dominant in the current NF market, the complicated production process during interfacial polymerization on porous substrates is one of their major drawbacks.[99] There are high market demands on integrally skinned asymmetric NF HFMs consisting of an ultrathin selective layer on a highly porous substrate made by NIPS or other strategies.

Chemically, PBI is a weakly basic polymer. It has a pK_a value of 5.5 in the protonated form[14] due to the fact that its heterocyclic imidazole group has two nitrogen atoms. The one attached to the H atom can be a hydrogen bond donor while the nitrogen with the lone pair is more likely to be a proton acceptor.[188] PBI may become self-charged in aqueous solutions since the adjacent benzene ring delocalizes the proton of the imidazole group. The self-charging feature can be used to directly develop PBI NF HFMs without additional modifications. Moreover, PBI-based NF membranes can overcome one major shortcoming of polyamide-based TFC NF membranes because the latter is vulnerable to chlorine attack during the chemical cleaning and disinfectant processes for water and wastewater treatment.[99]

Many research efforts have been devoted, since the early 2000s, to the fabrication of single- and dual-layer PBI-based NF HFMs through the NIPS process. Wang & Chung investigated the effects of bore fluid on the morphology and separation performance of PBI HFMs.[107,189] By using a mixture of DMAc and ethylene glycol as the bore fluid, the resultant PBI HFMs have no macrovoids in the inner substrate, as illustrated in Fig. 17. Therefore, the PBI HFMs could withstand a high operation pressure up to 30 bar. The asymmetric PBI NF HFMs had a PWP of 1.86 L m^{-2} h^{-1} bar^{-1}, a mean effective pore size of 0.348 nm in radius and a narrow pore size distribution. They could effectively segregate ions from salt mixtures because they had high rejections to divalent cations and anions while low rejections to monovalent ions. Clearly, the PBI NF HFMs can (1) remove heavy metals from wastewater and (2) separate chromate and sulfate ions from brines to facilitate the chlor-alkali process even under a high pH up to 14.[189,190] To further reduce the material cost and transport resistance but retain the high rejection characteristics, dual-layer PBI/PES NF HFMs were also developed.[191] The thickness of the PBI layer could be reduced to around 6 μm without compromising the separation performance. Therefore, both single- and dual-layer PBI NF HFMs have great potential to effectively remove heavy metal ions in various industries.

PBI based HFMs have also been explored in (1) forward osmosis (FO) for water reclamation[151,192–194] and protein concentration,[152] (2) pressure-retarded osmosis process (PRO) for power generation[139,195,196] and (3) organic solvent nanofiltration (OSN). Among them, PBI membranes for OSN have received most attention because most FO and PRO processes do not involve harsh environmental and testing conditions.

4.3 PBI HFMs for organic solvent nanofiltration (OSN)

OSN offers the most cutting-edge molecular-level separation and purification strategy in organic solvent media.[197–202] Although Sourirajan first proposed the concept of OSN in 1964 by using cellulose acetate membranes to separate liquid hydrocarbon mixtures,[203] it did not catch much attention because of the immaturity in membrane materials and technologies. Since the 2000s, the industrial demands on OSN have arisen swiftly due to (1) greater governmental and environmental regulations and (2) successful recovery of solvents from oil in the Max–Dewax process at ExxonMobil plants,[204] thus OSN membranes advanced rapidly with the aid of recently invented nanomaterials and membrane technologies. Today, OSN has proved its values as a promising energy-saving technology for (1) the recovery/reuse of organic solvents and (2) the concentration and recycle of valuable products such as catalysts, active pharmaceutical ingredients (APIs) and intermediates. Recently, catalyst-grafted PBI OSN organocatalytic membranes have been developed to be a sustainable membrane-based synthesis-separation platform for enantioselective organocatalysis.[205] As a process intensification methodology, the enhanced organocatalysis and compact reactor design reduced the E-factor and carbon footprint by 93% and 88%, respectively.

Although some lab-scale OSN HFMs have been made from chemically resistant or cross-linkable polymers, such as polyacrylonitrile (PAN),[206,207] polyphenylsulfone (PPSU),[208] polyimides/polyamides (*e.g.* P84,[209] Torlon,[210,211]), there are still no commercially available OSN HFMs for industrial applications. Since PBI already has limited dissolution in common solvents, the chemically crosslinked PBI should possess much higher chemical stability against plasticization and swelling in polar solvents. Moreover, different from the crosslinking modifications of PAN and polyimide membranes, the PBI backbone structure remains unchanged and strong after the modifications, making it a potential polymer to fabricate integrally skinned asymmetric OSN HFMs.

A dual-layer OSN HFM was synthesized by a coextrusion-crosslinking approach using PBI as the outer selective layer and *in situ* HPEI crosslinked P84 as the inner substrate layer.[145] The composite OSN HFM showed a rejection of >99% to methylene blue (MW: 319.85 g mol^{-1}) and good solvent permeances in water, methanol and MeCN. The chemical stability

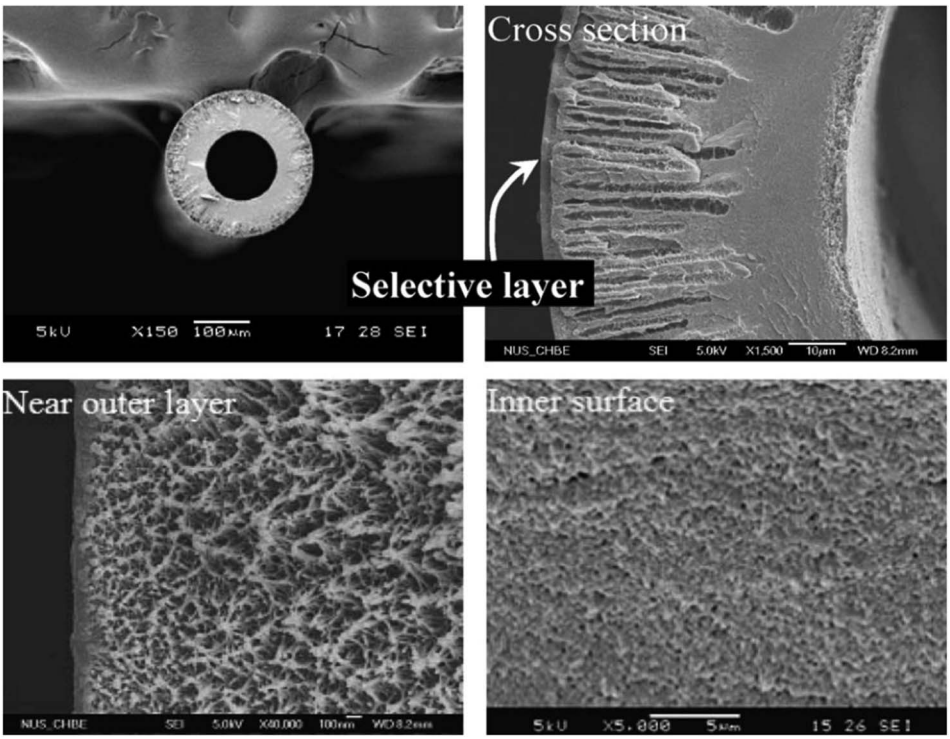

Fig. 17 Morphology of an asymmetric PBI nanofiltration hollow fiber membrane.Reproduced with permission from ref. 189, copyright 2006, Elsevier.

and selectivity of PBI membranes were largely improved in organic solvents. Tashvigh *et al.* synthesized acid-doped PBI HFMs after immersing them in a 2.0 wt% H_2SO_4/isopropanol solution.[42] The modified PBI membranes displayed remarkable stability in DMAc and DMF, fair stability in DMSO but poor stability in NMP due to the H-bonding between NMP and PBI which would weaken the performance of acid-doped PBI membranes. Therefore, doping PBI membranes with a strong acid might cause a leaching issue. By using a green cross-linking process, Zhao *et al.* modified PBI HFMs with a $K_2S_2O_8$ aqueous solution at 35 °C.[45] The resultant PBI membranes not only had greater stability in harsh solvents such as NMP, DMF and DMSO, but also showed better mechanical properties due to the newly formed N–N covalent bonds among different PBI chains. Wang *et al.* adopted a double modification strategy to fabricate integrally skinned PBI-DBX-SCA8 HFMs by combining DBX covalent crosslinking and 4-sulfocalix[8]arene (SCA8) ionic impregnation.[212] Synergistical improvements in chemical stability, molecular sieving ability and mechanical strength were observed. The PBI HFMs showed broad tolerance to polar, non-polar and aprotic polar solvents and had a controllable molecular-level separation ability. One-inch PBI HFM modules were also fabricated to demonstrate their long-term performance for solvent recovery from various acetone/oil mixtures.

4.4 PBI HFMs for pervaporation

Pervaporation is a membrane-based liquid separation that depends on the chemical potential difference (*i.e.*, partial vapor pressure) of components between the feed and permeate.[213] Generally, the upstream side of the membrane is in direct contact with the feed solution, while the downstream side is under vacuum or sweeping by an inert gas. The separation is achieved by the differences in solubilities and diffusivities of different volatile components across the membrane. Comparing with conventional liquid separations such as distillation and liquid–liquid extraction, pervaporation has higher separation efficiency, lower energy consumption, lower capital cost and less pollution.[214] It has been extensively used for solvent dehydration, separation of volatile organic compounds from wastewater, and separation of azeotropic or close boiling-point organic–organic mixtures in biorefinery, petrochemical, and pharmaceutical industries.[213–215] To achieve good permeability and selectivity, the ideal membrane for pervaporation must have strong chemical and thermal stability to survive in harsh environments.

Both single- and dual-layer PBI HFMs have been fabricated for pervaporation dehydration of organic solvents, such as ethylene glycol, acetone, ethyl acetate, phenol, alcohol, as well as organic–organic separation. Water can preferentially permeate across PBI membranes because it has a stronger affinity with PBI molecules and a smaller molecular size than most organic solvents. Wang *et al.* prepared single-layer PBI HFMs for the dehydration of ethylene glycol which showed much better separation performance in both permeance and separation factor than the PBI flat-sheet membranes.[106] However, the single-layer PBI HFMs had very low tensile properties and were too fragile to fabricate modules. Kung *et al.* fabricated blended PBI/Matrimid single-layer asymmetric

Table 5 PBI hollow fiber membranes for the dehydration of organic solvents and separation of solvent mixtures[a]

PBI hollow fiber membrane	Feed composition (wt%)	T (°C)	Flux (g m^{-2} h^{-1})	Separation factor	Ref.
m-PBI single-layer	Ethylene glycol/water (50/50)	60	1147	116 (water/EG)	Wang *et al.* 2010 (ref. 106)
m-PBI/P84 dual-layer	TFP/water (85/15)	60	332	1990 (water/TFP)	Wang *et al.* 2007 (ref. 141)
m-PBI/PEI dual layer thermally treated at 75 °C	Ethylene glycol/water (64/36)	60	186	4524 (water/EG)	Wang *et al.* 2010 (ref. 106)
m-PBI/PEI dual layer thermally treated at 75 °C	Ethylene glycol/water (80/20)	60	115	1763 (water/EG)	Wang *et al.* 2011 (ref. 149)
m-PBI/P84 dual-layer crosslinked by DCX and thermally treated at 250 °C	Acetone/water (85/15)	50	300	490 (water/acetone)	Shi *et al.* 2012 (ref. 142)
m-PBI single-layer crosslinked by DCX and thermal treated at 75 °C	Phenol/water (70/30)	60	196	722 (water/phenol)	Wang *et al.* 2014 (ref. 150)
m-PBI/PEI dual layer crosslinked by DCX	Ethyl acetate/water (98/2)	60	820	2478 (water/ethyl acetate)	Wang *et al.* 2015 (ref. 216)
m-PBI/Matrimid blend single-layer	Toluene/iso-octane (50/50)	60	1350	200 (toluene/iso-octane)	Kung *et al.* 2010 (ref. 158)

[a] DCX = *p*-xylene dichloride; P84 = BTDA-TDI/MDI co-polyimide; PEI = polyetherimide; TFP = tetrafluoropropanol.

HFMs for toluene/iso-octane separation by pervaporation.[158] The best performance was achieved with a flux of 1350 g m^{-2} h^{-1} and a separation factor of 200 using a toluene/iso-octane (50/50 wt%) mixture as the feed at a downstream pressure of 10 mbar.

To further improve the mechanical properties and separation performance of PBI HFMs, dual-layer PBI HFMs were made with the aid of co-extrusion spinning. P84 and PEI were chosen because they have excellent anti-swelling properties and good compatibility with PBI. The PBI/P84 dual-layer HFMs were fabricated for the dehydration of tetrafluoropropanol (TFP)[141] and acetone[142] using DCX cross-linked P84 as the porous substrate. Wang *et al.* used PEI as the inner support layer for ethylene glycol dehydration,[106,149] and achieved far better performance than most other polymeric membranes with a separation factor up to 4524 and a flux of 186 g m^{-2} h^{-1}. The PBI/PEI dual-layer HFMs were used for the dehydration of ethyl acetate and phenol. No delamination was observed at the interface between the two layers, indicating a good adhesion due to the miscibility of PBI and PEI.[150,216] Comparing with single-layer PBI HFMs, dual-layer PBI HFMs showed higher mechanical strength and flexibility. The dual-layer co-extrusion technology could also reduce the PBI material cost and enhance the overall separation performance. Therefore, there is great prospect in developing PBI dual-layer HFMs for pervaporation separations by using other robust but low-cost materials as substrates. A performance summary of PBI HFMs for the dehydration of organic solvents and separation of solvent mixtures is listed in Table 5. Clearly, the inherently rigid structure, high hydrophilicity and good spinnability make PBI a promising membrane material for pervaporation applications.

4.5 Gas separation for H_2/CO_2 separation at elevated temperatures

Polymeric membranes for conventional gas separations such as H_2/N_2, H_2/CO_2, O_2/N_2 and CO_2/CH_4 separations at or near ambient temperatures are well established.[33–35,217–220] Comparing with traditional gas separation technologies, such as solvent scrubbing, fractional/cryogenic distillation, liquid absorption, and pressure swing adsorption (PSA), membrane separation offers the advantages of high energy efficiency, small footprint, easy scale up, cost competitiveness and environmental friendliness. The demand for H_2 as an energy carrier for power generation is growing rapidly due to the global warming and climate changes. However pure hydrogen is not naturally available and must be produced from other sources.[221–224] Currently, methane steam reforming is the dominant route for large-scale hydrogen production because of the availability of natural gas. Through this process, synthesis gas (*i.e.*, syngas) which consists of H_2, CO, and unwanted CO_2 and H_2S, is produced from the reactions between methane and steam. The removal of CO_2 and H_2S from H_2 or their sequestration is critical for hydrogen to be a sustainable energy source. However, the presence of CO_2 and H_2S in the syngas stream at high temperatures makes the purification and separation technically and economically challenging. Although inorganic hydrogen-permeable membranes made of palladium and palladium alloys as well as ceramics have an impressively high selectivity for H_2 separation and can be operated at high temperatures,[225,226] they have the drawbacks of high costs and long-term stability issues such as embrittlement by hydrogen and performance deterioration due to the attack from sulfuric compounds.

Since polymeric membranes are relatively inexpensive, resistant to sulfur compounds, and can be easily fabricated into large-scale, defect-free membranes and modules, they may be particularly suitable for H_2 purification if the combustion turbines for power generation do not require high-purity H_2.[97] Unfortunately, most commercially available polymeric materials cannot withstand the high temperature of syngas exiting from the steam-reforming and water–gas shift reactions. The desirable polymeric membranes for syngas separation must be

Table 6 Overview of H_2/CO_2 separation performances of PBI hollow fiber membranes[a]

PBI hollow fiber membrane	Coating layer	Feed gas	ΔP	T (°C)		H_2 permeance (GPU)	H_2/CO_2 selectivity (−)	Ref.
PBI single layer	PBI-HFA	Pure	5–8 x 10^6 Pa (5–8 bar)	100	0.33	7.89	Kumbharkar *et al.* 2011	(ref. 81)
				200	0.62	12.83		
				300	0.99	21.74		
				400	2.60	27.28		
tert-butyl PBI single layer cross-linked by DBB	Silicone rubber	Pure	5–8 x 10^6 Pa (1–6 bar)	20	12.97	3.16	Kumbharkar & Li 2012	(ref. 232)
m-PBI/zirconia/stainless steel composite membrane	—	Pure	3.4 × 10^5 Pa (50 psia)	250	4.67	43.0	Berchtold *et al.* 2012	(ref. 233)
		Mixed syngas		250	7.00	47.6		
m-PBI single layer	Defect-seal layer	Pure	N/A	250 to 350	200–400	>20	Singh *et al.* 2014	(ref. 109)
m-PBI single layer	—	Pure	1.4 × 10^5 Pa (20 psia)	250	9.72	17.11	Dahe *et al.* 2019	(ref. 132)
				250	21.0	13.99		
				250	7.56	22.37		
m-PBI/PdNP single layer	—	Pure	1.0 × 10^5 Pa (1 bar)	60	80	10	Villalobos *et al.* 2018	(ref. 236)
m-PBI single layer	6F-PBI	Pure	1.4 × 10^5 Pa (20 psia)	95 to 350	90–400	>20	Singh *et al.* 2020	(ref. 82)
m-PBI single layer	Silicone rubber	Pure	7.0 × 10^5 Pa (7 bar)	150	65	17.6	Etxeberria-Benavides *et al.* 2020	(ref. 168)
m-PBI/10 wt% ZIF-8 single layer	Silicone rubber	Pure	7.0 × 10^5 Pa (7 bar)	150	107	16.1	Etxeberria-Benavides *et al.* 2020	(ref. 168)
PBI-HFA single layer	—	Pure	1.0 × 10^5 Pa (1 bar)	24	10 198	2.52	Kim *et al.* 2021	(ref. 237)
(*m*-PBI/10 wt% ZIF-8)/ Matrimid® 5218 dual-layer HFM	—	H_2/CO_2 50 : 50 (v/v)	7.0 × 10^5 Pa (7 bar)	180	64.5	12.3	Yang *et al.* 2012	(ref. 167)
(*m*-PBI/33 wt% ZIF-8)/ Matrimid® 5218 dual-layer HFM	—	H_2/CO_2 50 : 50 (v/v)	7.0 × 10^5 Pa (7 bar)	180	202	7.7	Yang *et al.* 2012	(ref. 167)
m-PBI:sPPSU (90 : 10)/ polysulfone dual-layer HFM cross-linked by DBX and thermally treated at 120 °C	—	H_2/CO_2 50 : 50 (v/v)	1.4 × 10^6 Pa (14 bar)	90	16.7	9.7	Naderi *et al.* 2019	(ref. 235)
Coating *m*-PBI on P84 HFM support	Silicone rubber	H_2/CO_2 50 : 50 (v/v)	6.0 × 10^5 Pa (6 bar)	180	39	20.2	Sánchez-Laínez *et al.* 2021	(ref. 234)

[a] 1 GPU = 1 × 10^{-6} cm^3 (STP) cm^{-2} s^{-1} $cmHg^{-1}$ = 7.50 × 10^{-12} m s^{-1} Pa^{-1}. DBB = 1,4-dibromobutane; DBX = α,α′-dibromo-*p*-xylene; P84 = BTDA-TDI/MDI co-polyimide; PdNPs = palladium nanoparticles; sPPSU = sulfonated polyphenylsulfone; ZIF-8 = zeolitic-imidazole framework-8.

mechanically, chemically, and thermally stable at high temperature and pressures.

Since H_2 has a smaller kinetic diameter than CO_2 (2.89 *vs.* 3.3 Å), the former has higher diffusivity than the latter. To design a membrane with high H_2/CO_2 selectivity, one must choose the polymers and operation conditions that (1) increase the diffusivity selectivity (favoring the H_2 permeate due to the size-sieving effect) and (2) suppress the solubility selectivity (favoring the condensable CO_2) as the governing factors for the entire gas transport.[73,168,227,228] In other words, the higher H_2/CO_2 selectivity arises from the combined effects: (1) H_2 shows higher diffusivity increase with temperature than CO_2 and (2) CO_2 has lower solubility at higher temperatures. Owing to the relatively rigid polymer chains, small free volume fraction and high T_g, PBI is one of the unique materials that has the above characteristics for effective H_2/CO_2 separation.

Although PBI has an extremely low flux for H_2 and CO_2 at room temperature, its rigid structure and high T_g offer the needed diffusivity-based selectivity at temperatures above 150 °C.[229] As the temperature increases, its H_2 permeance increases faster than CO_2 permeance, thereby increasing the H_2/CO_2 selectivity. The highly rigid PBI polymer chains also provide good resistance against CO_2- and SO_2-induced plasticization.[230,231] Table 6 summarizes the detailed H_2/CO_2 separation performance of recently developed PBI HFMs.[81,82,109,132,167,168,232–237] Key achievements and major breakthroughs are highlighted as follows.

Kumbharkar *et al.* fabricated *m*-PBI HFMs using DMAc/water as a bore fluid and water as an external coagulant and then coated them with 6F–PBI to seal the defects for H_2/CO_2 separation at 100–400 °C.[81] It was found that the bore fluid chemistry played an important role in determining membrane morphology, gas separation performance and mechanical strength. The resultant HFMs had a H_2 permeability of 2.6 GPU and a H_2/CO_2 selectivity of about 27 at 400 °C. Kumbharkar and Li also synthesized *tert*-butyl-PBI and fabricated it as asymmetric PBI HFMs using a dry-jet wet spinning approach.[232] The HFMs were crosslinked by 1,4-dibromobutane (DBB) and then dip coated with silicone rubber to seal the surface defects. Fig. 18 illustrates the crosslinking scheme between *tert*-butyl-PBI and DBB. The *tert*-butyl group substitution disrupted the PBI molecular chains and increased the FFV. Thus, the modified-PBI HFM membranes exhibited good separation performance for gas pairs such as CO_2/N_2, O_2/N_2 and H_2/N_2. For H_2/CO_2 separation, they had a higher H_2 permeance of 12.97 GPU but a lower H_2/CO_2 selectivity of 3.16 at 20 °C.

Berchtold *et al.* fabricated a PBI-stainless steel composite membrane by depositing a thin *m*-PBI layer through a proprietary process on the outer surface of a porous stainless-steel support consisting of an intermediate zirconia layer.[233] The

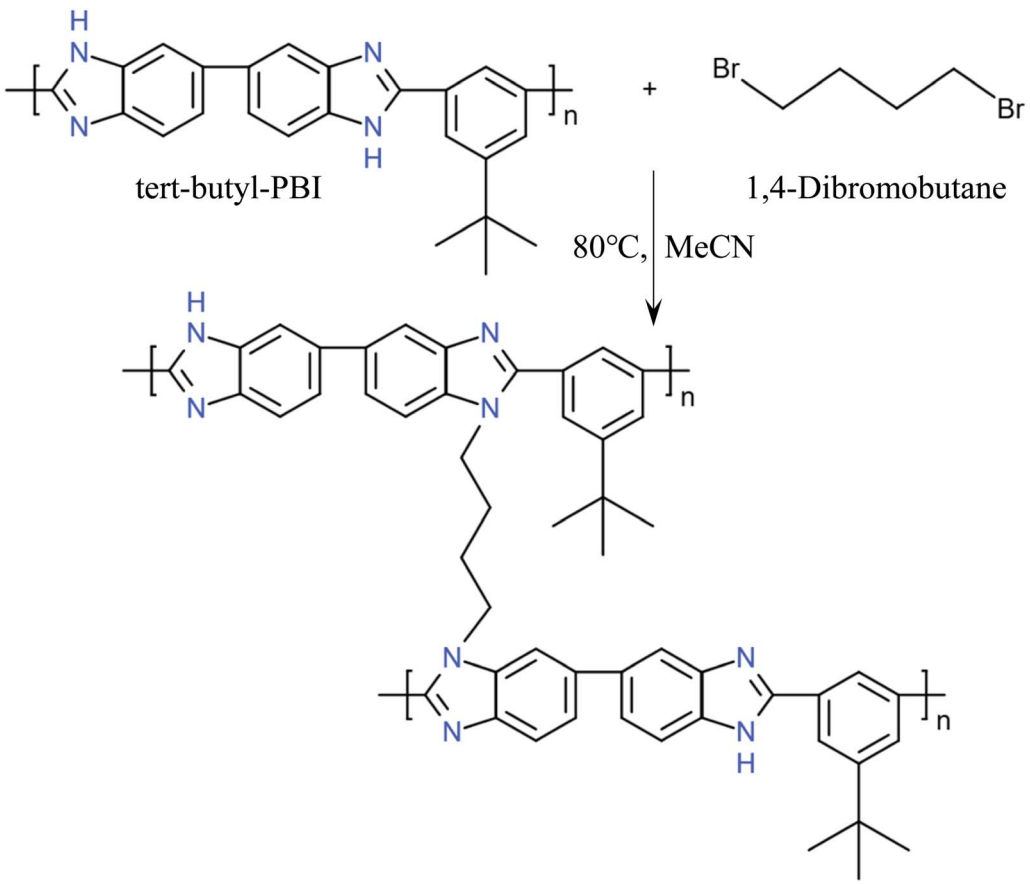

Fig. 18 The mechanism of crosslinking reaction between *tert*-butyl-PBI and DBB.[232]

PBI membrane module was tested for H_2/CO_2 separation from 150 to 250 °C in simulated dry syngas. It had a H_2 permeance and H_2/CO_2 selectivity of 7 GPU and 47 respectively at 250 °C, surpassing the 2008 Robeson's upper bound for H_2/CO_2 separation. Moreover, even in the presence of H_2S, the PBI composite membrane showed long-term stability without any performance degradation.

As mentioned in Section 3.2, both Dahe *et al.*[132] and Singh *et al.*[82] investigated the effect of coagulant chemistry on the removal of macrovoids from PBI HFM morphology. Today, the technologies to develop PBI HFMs with a highly interconnected and thermo-mechanically porous sub-layer have been established for H_2/CO_2 separations. Fig. 19 shows their typical morphology. After being annealed at 375 °C and coated with a 6F-PBI sealing layer, the resultant PBI HFMs showed commercially competitive permselectivity characteristics. They had a H_2 permeance of 200–400 GPU and a high ideal H_2/CO_2 selectivity of >20 at 250 to 350 °C.

In terms of PBI composite HFMs, Sánchez-Laínez prepared composite PBI/P84 HFMs by coating a thin PBI selective layer on a P84 HFM support using an *m*-PBI solution containing NaOH and ethanol.[234] After the silicone rubber coating, the PBI/P84 hollow fibers showed a H_2 permeance over 39 GPU with a H_2/CO_2 selectivity of 20.2 using a mixed H_2/CO_2 gas of 50 : 50 v/v as

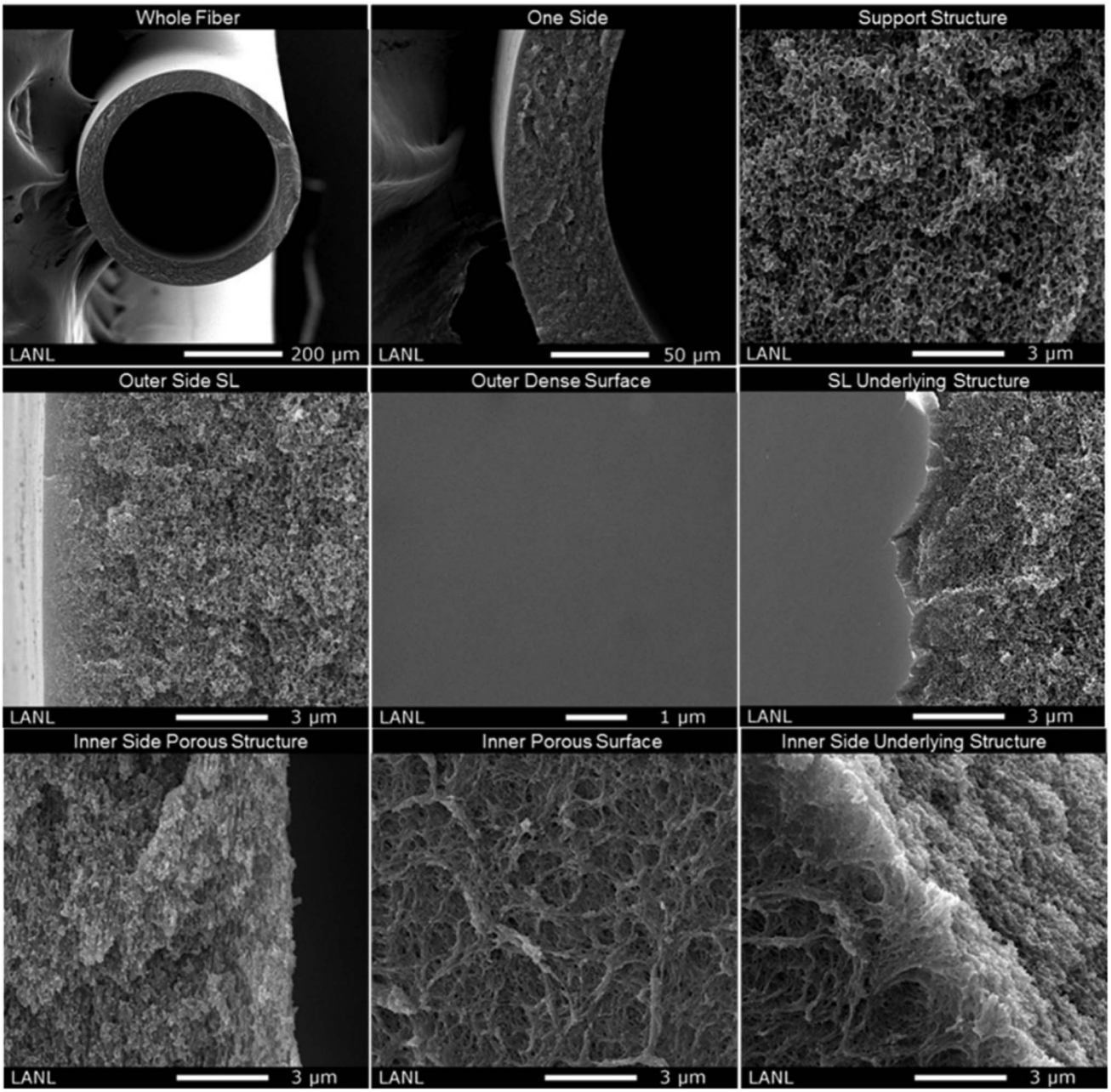

Fig. 19 Typical morphology of polybenzimidazole hollow fiber membranes for gas separation. Reproduced with permission from ref. 109, copyright 2014, Elsevier.

the feed at 7 bar and 180 °C. Naderi *et al.* fabricated dual-layer HFMs consisting of an outer-selective layer made of a PBI and sPPSU blend and a polysulfone inner-layer substrate.[235] sPPSU was chosen as an ionic-crosslinker so that the DBX modified PBI had a higher permeability than the pristine PBI. The resultant HFMs had a H_2 permeance of 16.7 GPU and an H_2/CO_2 selectivity of 9.7 at 90 °C and 14 bar.

PBI HFMs spun from MMMs were also developed using ZIFs as nanofillers. Yang *et al.* fabricated PBI/Matrimid dual-layer HFMs by incorporating ZIF-8 nanoparticles in the PBI selective layer.[167] The dual-layer HFMs were defect-free, without post-annealing and coating, but by optimizing ZIF-8 nanoparticle loadings, spinning conditions, and solvent-exchange procedures. When being tested at 180 °C using a H_2/CO_2 gas mixture (50 : 50 v/v) as the feed at 7 bar, two types of PBI HFMs were developed for hydrogen purification at high temperatures: (1) the HFMs containing 10 wt% ZIF-8 had a medium H_2 permeance of 64.5 GPU and a high selectivity of 12.3 and (2) the HFMs containing 33 wt% ZIF-8 had a high H_2 permeance of 202 GPU and a medium selectivity of 7.7. Moreover, the presence of CO and water vapor in the feed stream had no significant effects on membrane performance. Etxeberria-Benavides *et al.* fabricated defect-free PBI/ZIF-8 MMM HFMs comprising a thin dense layer of 300 nm by dispersing 10 wt% ZIF-8 into the PBI polymer matrix.[168] Comparing with pure PBI HFMs, the PBI MMM HFMs showed great increase in H_2 permeance from 65 GPU to 107 GPU at 150 °C and 7 bar, while the ideal H_2/CO_2 selectivity remained constant at 16.1. However, they found that the incorporation of ZIF-8 into the PBI polymer matrix could strongly influence gas transport, specifically in mixed gas tests. The enhanced H_2/CO_2 separation was compromised at high pressures of 30 bar owing to the strong CO_2 adsorption in the nanocavities of ZIF-8 that would suppress the H_2 transport.

With the aid of palladium nanoparticles (PdNPs), Villalobos *et al.* fabricated defect-free PBI/PdNP HFMs consisting of a thin dense skin layer filled with PdNPs by combining the complexation induced phase separation (CIPS) and NIPS processes,[236] as shown in Fig. 20. Palladium was added into the membrane in the form of ions to coordinate with the imidazole groups of PBI and minimize its agglomeration. The PBI/PdNP composite HFMs not only showed higher permeance than the pristine PBI membranes but also maintained the stability of Pd

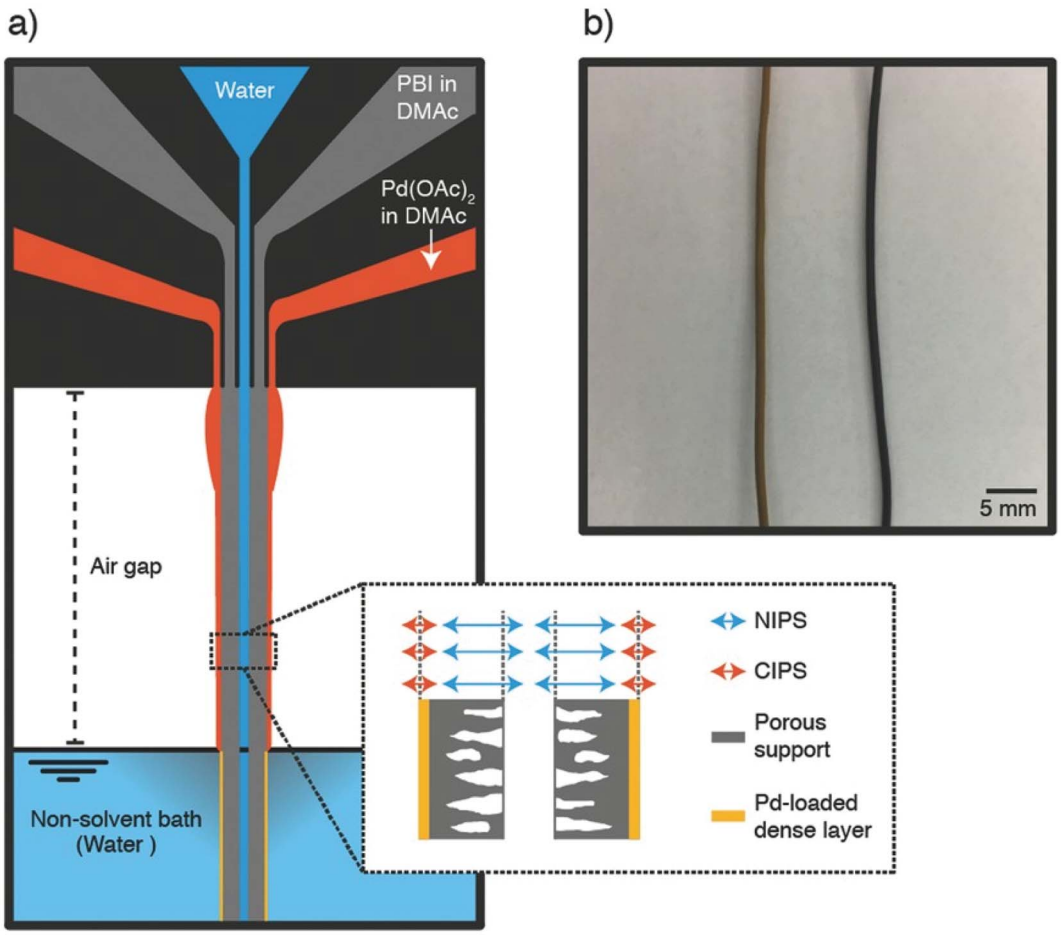

Fig. 20 Spinning process developed to make hollow fibers with a palladium-rich selective dense layer. (a) Diagram of the triple-orifice spinneret showing the orifice used for each solution and the two precipitation processes that take place (*i.e.*, CIPS and NIPS); (b) photograph of the PBI/PdNP hollow fiber before (left) and after (right) the reduction step to convert the Pd ions to PdNPs. Reproduced with permission from ref. 236, copyright 2018, John Wiley & Sons. Permission conveyed through Copyright Clearance Center, Inc.

nanoparticles due to the synergistic effects between PdNPs and the PBI matrix. The resultant PBI/PdNP HFMs made from a $Pd(OAc)_2$ concentration of 50×10^{-5} mol L^{-1} had a H_2 permeance and H_2/CO_2 selectivity of 80 GPU and 10 at 60 °C, respectively. As shown in Fig. 21, the performance of PBI hollow fiber membranes for H_2/CO_2 separation has gradually surpassed the upper bound of 2008 Robeson's curves.[65,238]

Other efforts have been made to (1) blend PBI with thermosets in order to improve the thermal stability,[239] (2) embed soluble organic macrocyclic cavitands (sulfocalixarenes, SCA) to form homogeneous PBI nanocomposite membranes with distinctly molecular-sieving nanocavities,[164,240] (3) grow a selective MOF layer on the PBI HFM surface,[241] (4) dope PBI membranes with a polyprotic acid to improve H_2/CO_2 diffusivity selectivity,[40] (5) apply Pd alloy (PdAg and PdNi) nanowires in PBI mixed matrix membranes to increase hydrogen diffusivity and reduce Pd embrittlement and susceptibility to poisoning,[242] (6) control the degree of *N*-quaternization on PBI based polymeric ionic liquids (PILs) to improve CO_2 sorption and gas permeation,[243] and (7) carbonize PBI as a carbon molecular sieve (CMS) with greatly enhanced H_2/CO_2, O_2/N_2 size-sieving ability.[244,245] These schemes may potentially enhance the separation performance of PBI-based HFMs if one can successfully and economically convert them from flat-sheet configurations to hollow fibers. Future studies should also be focused on their scalability, long-term performance, and techno-economic analyses for H_2/CO_2 separation at high temperatures.

5. Challenges and perspectives

As one of the engineering thermoplastics invented in the early 1960s, it took a much rougher pathway and a longer time for fully aromatic PBIs to reach market maturity and global attention compared to nylon or Teflon. Its unique characteristics such as extremely high temperature stability, oxidative resistance, chemical stability, and durability were too good to be used as an engineering polymer cost-effectively in the early days except in niche applications for aerospace, NASA mission and other harsh operation conditions. However, the deterioration of earth environments, water scarcity and pollution, and the demand for H_2 as an energy carrier for power generation have revitalized its importance. Today, PBI-based hollow fiber membranes have been found to have great potential and performance superiority in the fields of wastewater reuse and reclamation, organic solvent recovery, and efficient H_2 and CO_2 separation for hydrogen production and CO_2 capture. However, it is still a challenging research field in materials and processing, and the challenges are summarized as follows:

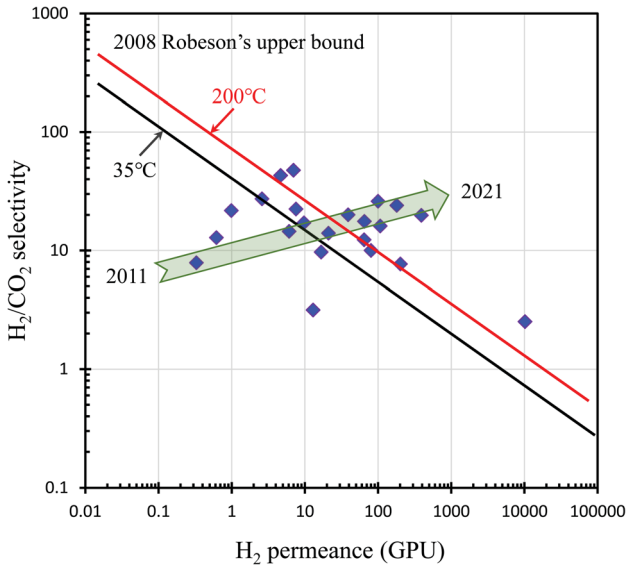

Fig. 21 Robeson's plot comparing the PBI hollow fiber membranes for H_2/CO_2 separation. The line represents the 2008 Robeson's upper bound.[65,238]

- Although advances in the fundamentals of single-layer hollow fiber formation and the state-of-the-art macrovoid-free PBI HFMs with an ultrathin dense-selective layer have been established, they are only applicable for the use of *m*-PBI (*i.e.*, commercially available Celazole® PBI). Since the optimal composition of the PBI-based dense-selective layer is still under extensive studies, it could be still a challenging task to design a defect-free integrally skinned asymmetric PBI HFM consisting of a tailored morphology and a tuneable dense-selective layer spun from MMMs or nanocomposite materials.
- The dual-layer co-extrusion technology should receive more attention in future R&D because it has the advantages of significantly reducing material costs and substructure resistance as well as enhancing the membrane's mechanical strength if a low-cost but robust material is employed as the support layer. So far, dual-layer PBI HFMs have demonstrated superior performance to single-layer ones in OSN and pervaporation as well as common gas separations at ambient temperature. Their applicability to H_2/CO_2 separation at high temperatures is a challenging task for further studies.
- The scalability, long-term performance, and techno-economic analyses of the aforementioned PBI HFMs must be conducted for actual industrial applications. This is especially imperative for H_2/CO_2 separation because (1) the methane steam reforming process produces syngas comprising multiple complicated components at high temperatures, and (2) the newly developed H_2-selective PBI-based HFMs have to survive in these harsh environments for a long period of operation time.
- To facilitate the commercialization of H_2-selective PBI-based HFMs for high-temperature applications, the highly permeable material 6F–PBI or PBI–HFA must be commercially available. Thus, similar to the use of silicone rubber materials to seal defects of conventional HFMs for O_2/N_2 and CO_4/CH_4 separations, a facile and cost-effective sealing procedure can be adopted for each PBI-based HFM for hydrogen recovery at high temperatures.

Molecular modelling and simulation have played an important role in advancing the fundamental understanding of membrane formation, material design and selection, and various separation mechanisms across membranes.[246–249] So far, the architecture designs of PBIs, PBI/nanocomposite materials and MMMs, and their membrane formation have not been exclusively examined at a molecular level. It is envisioned that

the combination of material simulation and advanced experiments may help build the relationships among polymer formulation, processing parameters, structural and mechanical analyses and separation performance that facilitate the development of next generation PBI-based membranes with precise separation. Given the unique and superior properties of PBI membranes, new demands for other separation methods may emerge for applications in the chemical, petrochemical, food, and pharmaceutical industries.

Conflicts of interest

There are no conflicts to declare.

Abbreviations

2-MeTHF	2-Methyl tetrahydrofuran
AEM	Anion exchange membrane
API	Active pharmaceutical ingredients
BDA	Butanediamine
BILP	Benzimidazole-linked polymer
CA	Cellulose acetate
CIPS	Complexation induced phase separation
CMS	Carbon molecular sieve
CO_2	Carbon dioxide
DAB	3,3′-Diaminobenzidine
DBB	1,4-Dibromobutane
DBX	α,α′-Dibromo-*p*-xylene
DCM	Dichloromethane
DCX	α,α′-Dichloro-*p*-xylene
DEO	1,2,7,8-Diepoxyoctane
DMAc	Dimethylacetamide
DMF	Dimethylformamide
DMSO	Dimethyl sulfoxide
ED	Electrodialysis
EG	Ethylene glycol
FFV	Fractional free volume
FO	Forward osmosis
GA	Glutaraldehyde
GO	Graphene oxide
HFA	4,4′-(Hexafluroisopropylidene)bis(benzoic acid)
HFM	Hollow fiber membrane
HPEI	Hyperbranched polyethyleneimine
IPN	Interpenetrating polymer network
ISA	Integrally skinned asymmetric
MBRs	Membrane bioreactors
MCDI	Membrane capacitive deionization
MeCN	Acetonitrile
MF	Microfiltration
MMM	Mixed matrix membrane
MOF	Metal–organic frameworks
MPC	Metal–polymer coordination
MW	Molecular weight
MWCO	Molecular weight cut off
NASA	National Aeronautics and Space Administration
NF	Nanofiltration
NIPS	Non-solvent induced phase inversion or separation
NMP	*N*-Methyl-2-pyrrolidone
NS	Non-solvent
OSN	Organic solvent nanofiltration
P84	Co-polyimide, BTDA-TDI/MDI
PAN	Polyacrylonitrile
PBI	Polybenzimidazole
PBI-OH	Hydroxylated polybenzimidazole
PDA	Polydopamine
PdNPs	Palladium nanoparticles
PEI	Polyetherimide
PEM	Polymer electrolyte membranes
PES	Polyethersulfone
PI	Polyimide
PILs	Polymeric ionic liquids
PIM	Polymer of intrinsic microporosity
POF	Porous organic framework
POSS	Polyhedral oligomeric silsesquioxane
PPA	Polyphosphoric acid
PPL	Polypyrrolone
PPMA	Phosphorus pentoxide/methanesulfonic acid
PPSU	Polyphenylsulfone
PRO	Pressure-retarded osmosis process
PSA	Pressure swing adsorption
RO	Reverse osmosis
SG	Sulfonated graphene
sPPSU	Sulfonated polyphenylsulfone
TAPDS	Tetraaminodiphenylsulfone
TBB	1,3,5-Tris(bromomethyl)benzene
TCL	Terephthaloyl chloride
TDI	Toluene 2,4-diisocyanate
TFC	Thin film composite
TFP	Tetrafluoropropanol
TG	Glass transition temperature
TGIC	Triglycidylisocyanurate
THF	Tetrahydrofuran
TMC	Trimesoyl chloride
UF	Ultrafiltration
XDA	*p*-Xylenediamine
ZIF	Zeolitic imidazolate frameworks

Nomenclature

δ_T	Total solubility parameter of a material
δ_d	Solubility parameter contributed by dispersion forces
δ_p	Solubility parameter contributed by polar interactions
δ_h	Solubility parameter contributed by hydrogen bonding

Acknowledgements

The authors would like to express their gratitude to BASF SE, Germany for the financial support of the grant (R-279-000-411-597). Thanks are due to PBI performance Products Inc. (USA) for providing PBI dopes. Prof Chung would also like to thank the Ministry of Science and Technology, Taiwan for Grant/Award Number of MOST 110-2222-E-011-022-MY3 and the

Yushan Scholar Program supported by the Ministry of Education, Taiwan. Thanks are also due to Prof. Wang Yan from University Huazhong University of Science and Technology for her valuable suggestions.

References

1 H. Vogel and C. S. Marvel, *J. Polym. Sci.*, 1961, **50**, 511–539.
2 D. R. Coffin, G. A. Serad, H. L. Hicks and R. T. Montgomery, *Text. Res. J.*, 1982, **52**, 466–472.
3 D. A. Chatfield and I. N. Einhorn, *J. Polym. Sci. Polym. Chem. Ed.*, 1981, **19**, 601–618.
4 E. W. Neuse, *Adv. Polm. Sci.*, 1982, **47**, 1.
5 E. D. Powers and G. A. Serad, in *High Performance Polymers: Their Origin and Development,* ed. R. B. Seymour and G. S. Kirshenbaum, Elsevier, New York, 1986.
6 A. Buckley, D. Stuetz and G. A. Serad, in *Encycl. Polym. Sci. Eng.*, ed. J. I. Kroschwitz, Wiley, New York, 1987.
7 M. Ueda, M. Sato and A. Mochizuki, *Macromolecules*, 1985, **18**, 2723–2726.
8 J. P. Critchley, G. J. Knight and W. W. Wright, in *Heat-Resistance Polym*. Plenum Press. New York, 1983.
9 T. S. Chung, *J. Macromol. Sci., Polym. Rev.*, 1997, **37**, 277–301.
10 Y. Wang, T. X. Yang, K. Fishel, B. C. Benicewicz and T. S. Chung, in *Handbook of Thermoplastics*, ed. O. Olabisi and K. Adewale, CRC Press, 2th edn, 2016, pp.617–667.
11 S. Cong, J. Wang, Z. Wang and X. Liu, *Green Chem. Eng.*, 2021, **2**, 44–56.
12 A. Kausar, *Polym-Plast. Technol. Mater.*, 2019, **58**, 1979–1992.
13 J. T. Wang, R. F. Savinell, J. Wainright, M. Litt and H. Yu, *Electrochim. Acta*, 1996, **41**, 193–197.
14 Z. Zhou, O. Zholobko, X. F. Wu, T. Aulich, J. Thakare and J. Hurley, *Energies*, 2021, **14**, 135.
15 Q. Li, R. He, J. O. Jensen and N. J. Bjerrum, *Fuel Cells*, 2004, **4**, 147–159.
16 L. Xiao, H. Zhang, E. Scanlon, L. S. Ramanathan, E. W. Choe, D. Rogers, T. Apple and B. C. Benicewicz, *Chem. Mater.*, 2005, **17**, 5328–5333.
17 J. S. Wainright, J.-T. Wang, D. Weng, R. F. Savinell and M. Litt, *J. Electrochem. Soc.*, 1995, **142**, L121.
18 P. Wang, J. Peng, B. Yin, X. Fu, L. Wang, J. L. Luo and X. Peng, *J. Mater. Chem. A*, 2021, **9**(46), 26345–26353.
19 X. Li, H. Ma, P. Wang, Z. Liu, J. Peng, W. Hu, Z. Jiang, B. Liu and M. D. Guiver, *Chem. Mater.*, 2020, **32**(3), 1182–1191.
20 A. Kalathil, A. Raghavan and B. Kandasubramanian, *Polym. Technol. Mater.*, 2019, **58**, 465–497.
21 J. Mader, L. Xiao, T. J. Schmidt, B. Fuel and V. Ave, *Adv. Polm. Sci.*, 2008, **216**, 63–124.
22 S. Yu and B. C. Benicewicz, *Macromolecules*, 2009, **42**, 8640–8648.
23 T. D. Dang, N. Venkat and J. E. Mark, in *Polyimides Other High-Temperature Polymers: Synthesis, Characterization and Applications*, ed. K. L. Mittal, 2009.
24 J. Escorihuela, J. Olvera-Mancilla, L. Alexandrova, L. F. del Castillo and V. Compañ, *Polymers*, 2020, **12**, 1861.
25 D. Aili, D. Henkensmeier, S. Martin, B. Singh, Y. Hu, J. O. Jensen, L. N. Cleemann and Q. Li, *Electrochem. Energy Rev.*, 2020, **3**, 793–845.
26 Y. Sui, H. Hu, M. Ueda, L. Wang and X. Zhang, *J. Memb. Sci.*, 2019, **572**, 262–270.
27 X. Wang, W. Chen, T. Li, X. Yan, Y. Zhang, F. Zhang, X. Wu, B. Pang, J. Li and G. He, *J. Mater. Chem. A*, 2021, **9**, 7522–7530.
28 M. Guo, T. Ban, Y. Wang, Y. Wang, Y. Zhang, J. Zhang and X. Zhu, *J. Membr. Sci.*, 2022, **647**, 120299.
29 L. Cseri, J. Baugh, A. Alabi, A. Alhajaj, L. Zou, R. Dryfe, P. M. Budd and G. Szekely, *J. Mater. Chem. A*, 2018, **6**(48), 24728–24739.
30 R. McNair, L. Cseri, G. Szekely and R. Dryfe, *ACS Appl. Polym. Mater.*, 2020, **2**(7), 2946–2956.
31 S. Loeb and S. Sourirajan, Saline Water Conversion-II, *Adv. Chem.*, 1963, **38**, 117–132.
32 R. W. Baker and K. Lokhandwala, *Ind. Eng. Chem. Res.*, 2008, **47**, 2109–2121.
33 D. S. Sholl and R. P. Lively, *Nature*, 2016, **532**, 435–437.
34 R. P. Lively and D. S. Sholl, *Nat. Mater.*, 2017, **16**, 276–279.
35 N. Peng, N. Widjojo, P. Sukitpaneenit, M. M. Teoh, G. G. Lipscomb, T. S. Chung and J. Y. Lai, *Prog. Polym. Sci.*, 2012, **37**, 1401–1424.
36 K. P. Bye, V. Loianno, T. N. Pham, R. Liu, J. S. Riffle and M. Galizia, *J. Memb. Sci.*, 2019, **580**, 235–247.
37 A. A. Tashvigh, Y. Feng, M. Weber, C. Maletzko and T. S. Chung, *Ind. Eng. Chem. Res.*, 2019, **58**, 10678–10691.
38 C. Marquié, *J. Agric. Food Chem.*, 2001, **49**, 4676–4681.
39 D. Y. Xing, S. Y. Chan and T. S. Chung, *Green Chem.*, 2014, **16**, 1383–1392.
40 L. Zhu, M. T. Swihart and H. Lin, *Energy Environ. Sci.*, 2018, **11**, 94–100.
41 Y. Wang, T. S. Shung and M. Gruender, *J. Memb. Sci.*, 2012, **416**, 486–495.
42 A. A. Tashvigh and T. S. Chung, *J. Memb. Sci.*, 2019, **572**, 580–587.
43 J. Hu, R. Hardian, M. Gede, T. Holtzl and G. Szekely, *J. Memb. Sci.*, 2022, **648**, 120383.
44 D. Chen, C. Yan, X. Li, L. Liu, D. Wu and X. Li, *Sep. Purif. Technol.*, 2019, **224**, 15–22.
45 B. Zhao, G. M. Shi, K. Y. Wang, J. Y. Lai and T. S. Chung, *Sep. Purif. Technol.*, 2021, **255**, 117702.
46 G. Ignacz, F. Fei and G. Szekely, *ACS Applied Nano Materials*, 2018, **1**(11), 6349–6356.
47 R. Hardian, P. Pogany, Y. M. Lee and G. Szekely, *J. Mater. Chem. A*, 2021, **9**(25), 14400–14410.
48 J. Lee, H. Yang and T. H. Bae, *Membranes*, 2022, **12**(2), 140.
49 K. Y. Wang, Y. Xiao and T. S. Chung, *Chem. Eng. Sci.*, 2006, **61**, 5807–5817.
50 K. Y. Wang, Q. Yang, T. S. Chung and R. Rajagopalan, *Chem. Eng. Sci.*, 2009, **64**, 1577–1584.
51 D. Chen, S. Yu, M. Yang, D. Li and X. Li, *RSC Adv.*, 2016, **6**, 16925–16932.
52 I. B. Valtcheva, S. C. Kumbharkar, J. F. Kim, Y. Bhole and A. G. Livingston, *J. Memb. Sci.*, 2014, **457**, 62–72.

53 I. B. Valtcheva, P. Marchetti and A. G. Livingston, *J. Memb. Sci.*, 2015, **493**, 568–579.
54 A. Oxley, P. R. Gaffney, D. Kim, P. Marchetti and A. G. Livingston, *J. Memb. Sci.*, 2022, **647**, 120199.
55 A. A. Tashvigh, L. Luo, T. S. Chung, M. Weber and C. Maletzko, *J. Memb. Sci.*, 2018, **551**, 204–213.
56 A. A. Tashvigh and T. S. Chung, *J. Memb. Sci.*, 2018, **560**, 115–124.
57 M. H. D. A. Farahani and T. S. Chung, *Sep. Purif. Technol.*, 2018, **209**, 182–192.
58 F. Fei, L. Cseri, G. Szekely and C. F. Blanford, *ACS Appl. Mater. Interfaces*, 2018, **10**, 16140–16147.
59 J. R. Potts, D. R. Dreyer, C. W. Bielawski and R. S. Ruoff, *Polymer*, 2011, **52**, 5–25.
60 D. Zhao, J. F. Kim, G. Ignacz, P. Pogany, Y. M. Lee and G. Szekely, *ACS Nano*, 2019, **13**, 125–133.
61 F. Fei, H. A. Le Phuong, C. F. Blanford and G. Szekely, *ACS Applied Polymer Materials*, 2019, **1**(3), 452–460.
62 S. D. Kim, G. Y. Won, A. A. Shah, A. Park, Y. I. Park, S. E. Nam, Y. H. Cho and H. Park, *J. Memb. Sci*, 2021, **636**, 119587.
63 A. Alammar, S. H. Park, C. J. Williams, B. Derby and G. Szekely, *J. Membr. Sci.*, 2020, **603**, 118007.
64 L. Zhu, M. T. Swihart and H. Lin, *J. Mater. Chem. A*, 2017, **5**, 19914–19923.
65 L. M. Robeson, *J. Memb. Sci.*, 2008, **320**, 390–400.
66 A. Naderi, A. A. Tashvigh and T. S. Chung, *J. Memb. Sci.*, 2019, **572**, 343–349.
67 S. S. Hosseini, M. M. Teoh and T. S. Chung, *Polymer*, 2008, **49**, 1594–1603.
68 H. W. Yoon, Y. H. Cho and H. B. Park, Graphene-based membranes: status and prospects, *Phil. Trans. R. Soc. A*, 2016, **374**, 20150024.
69 J. Shen, G. Liu, Y. Ji, Q. Liu, L. Cheng, K. Guan, M. Zhang, G. Liu, J. Xiong, J. Yang and W. Jin, *Adv. Funct. Mater.*, 2018, **28**, 1801511.
70 Y. Jin, B. Gao, C. Bian, X. Meng, B. Meng, S. I. Wong, N. Yang, J. Sunarso, X. Tan and S. Liu, *Green Chem.*, 2021, **23**, 3374–3385.
71 N. P. Panapitiya, S. N. Wijenayake, D. D. Nguyen, Y. Huang, I. H. Musselman, K. J. Balkus Jr and J. P. Ferraris, *ACS Appl. Mater. Interfaces*, 2015, **7**, 18618–18627.
72 K. A. Stevens, J. D. Moon, H. Borjigin, R. Liu, R. M. Joseph, J. S. Riffle and B. D. Freeman, *J. Memb. Sci.*, 2020, **593**, 117427.
73 X. Li, R. P. Singh, K. W. Dudeck, K. A. Berchtold and B. C. Benicewicz, *J. Memb. Sci.*, 2014, **461**, 59–68.
74 S. C. Kumbharkar, P. B. Karadkar and U. K. Kharul, *J. Memb. Sci.*, 2006, **286**, 161–169.
75 M. A. Abdulhamid, R. Hardian, P. M. Bhatt, S. J. Datta, A. Ramirez, J. Gascon, M. Eddaoudi and G. Szekely, *Applied Materials Today*, 2022, **26**, 101271.
76 J. R. Klaehn, C. J. Orme and E. S. Peterson, *J. Memb. Sci.*, 2016, **515**, 1–6.
77 X. Li, G. Qian, X. Chen and B. C. Benicewicz, *Fuel Cells*, 2013, **13**, 832–842.
78 M. B. Moe, W. J. Koros and D. R. Paul, *J. Polym. Sci. Part B: Polym. Phys.*, 1988, **26**, 1931–1945.
79 M. W. Hellums, W. J. Koros, G. R. Husk and D. R. Paul, *J. Memb. Sci.*, 1989, **46**, 93–112.
80 S. C. Kumbharkar, M. N. Islam, R. A. Potrekar and U. K. Kharul, *Polymer*, 2009, **50**, 1403–1413.
81 S. C. Kumbharkar, Y. Liu and K. Li, *J. Memb. Sci.*, 2011, **375**, 231–240.
82 R. P. Singh, G. J. Dahe, K. W. Dudeck and K. A. Berchtold, *Int. J. Hydrogen Energy*, 2020, **45**, 27331–27345.
83 R. P. Singh, X. Li, K. W. Dudeck, B. C. Benicewicz and K. A. Berchtold, *Polymer*, 2017, **119**, 134–141.
84 S. H. Han, J. E. Lee, K. J. Lee, H. B. Park and Y. M. Lee, *J. Memb. Sci.*, 2010, **357**, 143–151.
85 H. Borjigin, K. A. Stevens, R. Liu, J. D. Moon, A. T. Shaver, S. Swinnea, B. D. Freeman, J. S. Riffle and J. E. Mcgrath, *Polymer*, 2015, **71**, 135–142.
86 S. C. Kumbharkar and U. K. Kharul, *Eur. Polym. J.*, 2009, **45**, 3363–3371.
87 S. C. Kumbharkar and U. K. Kharul, *J. Memb. Sci.*, 2010, **357**, 134–142.
88 M. G. Rabbani and H. M. El-Kaderi, *Chem. Mater.*, 2011, **23**, 1650–1653.
89 A. K. Sekizkardes, J. T. Culp, T. Islamoglu, A. Marti, D. Hopkinson, C. Myers, H. M. El-Kaderi and H. B. Nulwala, *Chem. Commun.*, 2015, **51**, 13393–13396.
90 M. Shan, X. Liu, X. Wang, I. Yarulina, B. Seoane, F. Kapteijn and J. Gascon, *Sci. Adv.*, 2018, **4**, eaau1698.
91 X. Wang, M. Shan, X. Liu, M. Wang, C. M. Doherty, D. Osadchii and F. Kapteijn, *ACS Appl. Mater. Interfaces*, 2019, **11**, 20098–20103.
92 M. Mulder, *Basic Principles of Membrane Technology*, Kluwer Academic. Boston, 1996.
93 H. Tompa, *Polymer Solutions*, Butterworths Scientific Publications. London, 1956.
94 H. Strathmann, P. Scheible and R. W. Baker, *J. Appl. Polym. Sci.*, 1971, **15**, 811–828.
95 G. R. Guillen, Y. Pan, M. Li and E. M. V Hoek, *Ind. Eng. Chem. Res.*, 2011, **50**, 3798–3817.
96 *Hollow Fiber Membranes: Fabrication and Applications*. ed. T.S. Chung and Y. Feng, Elsevier, 2021.
97 R. W. Baker, *Membrane Technology and Applications*. John Wiley & Sons, 2012.
98 R. P. Lively, M. E. Dose, L. Xu, J. T. Vaughn, J. R. Johnson, J. A. Thompson, K. Zhang, M. E. Lydon, J.-S. Lee, L. Liu, Z. Hu, O. Karvan, M. J. Realff and W. J. Koros, *J. Membr. Sci.*, 2012, **423–424**, 302–313.
99 G. M. Urper, R. Sengur-Tasdemir, T. Turken, E. A. Genceli, V. V Tarabara and I. Koyuncu, *Sep. Purif. Technol.*, 2017, **52**, 2120–2136.
100 H. V. Samuelson, *US Pat.*,4861661, 1989.
101 S. Husain and W. J. Koros, *J. Memb. Sci.*, 2007, **288**, 195–207.
102 M. F. A. Wahab, A. F. Ismail and S. J. Shilton, *Sep. Purif. Technol.*, 2012, **86**, 41–48.
103 F. S. Model, H. J. Davis and J. E. Poist, *PBI Membrane for Reverse Osmosis*, ed. S. Sourirajan, Reverse Osmosis Synth. Membr, Ottawa, 1977, p. 231.

104 A. M. Striegel, *J. Chil. Chem. Soc.*, 2003, **48**, 73–77.
105 C. B. Shogbon, J. L. Brousseau, H. Zhang, B. C. Benicewicz and Y. A. Akpalu, *Macromolecules*, 2006, **39**, 9409–9418.
106 Y. Wang, M. Gruender and T. S. Chung, *J. Memb. Sci.*, 2010, **363**, 149–159.
107 K. Y. Wang and T. S. Chung, *AIChE J.*, 2006, **52**, 1363–1377.
108 N. Widjojo and T. S. Chung, *Ind. Eng. Chem. Res.*, 2006, **45**, 7618–7626.
109 R. P. Singh, G. J. Dahe, K. W. Dudeck, C. F. Welch and K. A. Berchtold, *Energy Procedia*, 2014, **63**, 153–159.
110 C. Cohen, G. B. Tanny and S. Prager, *J. Polym. Sci. Polym. Phys.*, 1979, **17**, 477–489.
111 A. J. Reuvers, J. W. A. van den Berg and C. A. Smolders, *J. Memb. Sci.*, 1987, **34**, 45–65.
112 C. A. Smolders, A. J. Reuvers, R. M. Boom and I. M. Wienk, *J. Memb. Sci.*, 1992, **73**, 259–275.
113 H. Strathmann, K. Kock, P. Amar and R. W. Baker, *Desalination*, 1975, **16**, 179.
114 H. Strathmann and K. Kock, The formation mechanism of phase inversion membranes, *Desalination*, 1977, **21**, 241–255.
115 V. G. Levich and V. S. Krylov, *Annu. Rev. Fluid. Mech.*, 1969, **1**, 293–316.
116 S. A. McKelvey and W. J. Koros, *J. Memb. Sci.*, 1996, **112**, 29–39.
117 M. R. Pekny, A. R. Greenberg, V. Khare, J. Zartman, W. B. Krantz and P. Todd, *J. Memb. Sci.*, 2002, **205**, 11–21.
118 M. R. Pekny, J. Zartman, W. B. Krantz, A. R. Greenberg and P. Todd, *J. Memb. Sci.*, 2003, **211**, 71–90.
119 M. A. Frommer and R. M. Messalem, *Ind. Eng. Chem. Prod. Res. Dev.*, 1973, **12**, 328–333.
120 N. Peng, T. S. Chung and K. Y. Wang, *J. Memb. Sci.*, 2008, **318**, 363–372.
121 K. Y. Lin, D. M. Wang and J.-Y. Lai, *Macromolecules*, 2002, **35**, 6697–6706.
122 Y. Liu, G. H. Koops and H. Strathmann, *J. Memb. Sci.*, 2003, **223**, 187–199.
123 A. J. Reuvers, F. W. Altena and C. A. Smolders, *J. Polym. Sci. Part B: Polym. Phys.*, 1986, **24**, 793–804.
124 D. M. Wang, F. C. Lin, T. T. Wu and J. Y. Lai, *J. Memb. Sci.*, 1998, **142**, 191–204.
125 N. Peng, T. S. Chung and J. Y. Lai, *J. Memb. Sci.*, 2009, **326**, 608–617.
126 T. S. Chung and E. R. Kafchinski, *J. Appl. Polym. Sci.*, 1997, **65**, 1555–1569.
127 K. Y. Wang, D. F. Li, T. S. Chung and S. B. Chen, *Chem. Eng. Sci.*, 2004, **59**, 4657–4660.
128 K. Y. Wang, T. Matsuura, T. S. Chung and W. F. Guo, *J. Memb. Sci.*, 2004, **240**, 67–79.
129 A. K. Hołda and I. F. J. Vankelecom, *J. Appl. Polym. Sci.*, 2015, **132**, 1–17.
130 C. M. Hansen, *Hansen Solubility Parameters: A User's Handbook*, CRC Press, 2007.
131 D. W. van Krevelen and K. Te Nijenhuis, *Properties of Polymers: Their Correlation with Chemical Structure; Their Numerical Estimation and Prediction from Additive Group Contributions*, Elsevier Science, 4th edn, 2009.
132 G. J. Dahe, R. P. Singh, K. W. Dudeck, D. Yang and K. A. Berchtold, *J. Memb. Sci.*, 2019, **577**, 91–103.
133 W. Henne, G. Dunweg, W. Schmitz, R. Pohle and F. Lawitzki, *US Pat.*, 4164437A, 1979.
134 D. F. Li, T. S. Chung, R. Wang and Y. Liu, *J. Memb. Sci.*, 2002, **198**, 211–223.
135 H. Suzuki, K. Tanaka, H. Kita, K. Okamoto, H. Hoshino, T. Yoshinaga and Y. Kusuki, *J. Memb. Sci.*, 1998, **146**, 31–37.
136 N. Widjojo, T. S. Chung and W. B. Krantz, *J. Memb. Sci.*, 2007, **294**, 132–146.
137 D. Bhandari, K. O. Olanrewaju, N. Bessho and V. Breedveld, *Sep. Purif. Technol.*, 2013, **104**, 68–80.
138 T. He, M. H. V. Mulder, H. Strathmann and M. Wessling, *J. Memb. Sci.*, 2002, **207**, 143–156.
139 F.-J. Fu, S. Zhang, S. P. Sun, K. Y. Wang and T. S. Chung, *J. Memb. Sci.*, 2013, **443**, 144–155.
140 L. Setiawan, L. Shi and R. Wang, *Polymer*, 2014, **55**, 1367–1374.
141 K. Y. Wang, T. S. Chung and R. Rajagopalan, *J. Memb. Sci.*, 2007, **287**, 60–66.
142 G. M. Shi, Y. Wang and T. S. Chung, *AIChE J.*, 2012, **58**, 1133–1145.
143 Y. K. Ong and T. S. Chung, *AIChE J.*, 2013, **59**, 3006–3018.
144 L. Y. Jiang, H. M. Chen, Y. C. Jean and T. , S. Chung, *AIChE J.*, 2009, **55**, 75–86.
145 S. P. Sun, S. Y. Chan, W. Xing, Y. Wang and T. S. Chung, *ACS Sustain. Chem. Eng.*, 2015, **3**, 3019–3023.
146 S. P. Sun, S. Y. Chan and T. S. Chung, *Chem. Eng. Sci.*, 2015, **129**, 232–242.
147 Z. Y. Wang, Z. J. Fu, D. D. Shao, M. J. Lu, Q. C. Xia, H. F. Xiao, B. W. Su and S. P. Sun, *J. Memb. Sci.*, 2020, **610**, 118270.
148 H. Dzinun, M. H. D. Othman, A. F. Ismail, M. H. Puteh, M. A. Rahman and J. Jaafar, *J. Memb. Sci.*, 2015, **479**, 123–131.
149 Y. Wang, T. S. Chung, W. B. Neo and M. Gruender, *J. Memb. Sci.*, 2011, **378**, 339–350.
150 Y. Wang, M. Gruender and S. Xu, *Ind. Eng. Chem. Res.*, 2014, **53**, 18291–18303.
151 Q. Yang, K. Y. Wang and T. S. Chung, *Environ. Sci. Technol.*, 2009, **43**, 2800–2805.
152 Q. Yang, K. Y. Wang and T. S. Chung, *Sep. Purif. Technol.*, 2009, **69**, 269–274.
153 D. T. Clausi and W. J. Koros, *J. Membr. Sci.*, 2000, **167**, 79–89.
154 J. J. Krol, M. Boerrigter and G. H. Koops, *J. Memb. Sci.*, 2001, **184**, 275–286.
155 T. K. Ahn, M. Kim and S. Choe, *Macromolecules*, 1997, **30**, 3369–3374.
156 E. Földes, E. Fekete, F. E. Karasz and B. Pukánszky, *Polymer*, 2000, **41**, 975–983.
157 T. S. Chung, Z.-L. Xu and C. H. A. Huan, *J. Polym. Sci. Part B Polym. Phys.*, 1999, **37**, 1575–1585.
158 G. Kung, L. Y. Jiang, Y. Wang and T. S. Chung, *J. Memb. Sci.*, 2010, **360**, 303–314.
159 Z.-L. Xu, T. S. Chung, K.-C. Loh and B. Chun, *J. Memb. Sci.*, 1999, **158**, 41–53.

160 T. S. Chung, L. Y. Jiang, Y. Li and S. Kulprathipanja, *Prog. Polym. Sci.*, 2007, **32**, 483–507.
161 G. Liu, V. Chernikova, Y. Liu, K. Zhang, Y. Belmabkhout, O. Shekhah, C. Zhang, S. Yi, M. Eddaoudi and W. J. Koros, *Nat. Mater.*, 2018, **17**, 283–289.
162 R. Mahajan, R. Burns, M. Schaeffer and W. J. Koros, *J. Appl. Polym. Sci.*, 2002, **86**, 881–890.
163 G. Dong, H. Li and V. Chen, *J. Mater. Chem. A*, 2013, **1**, 4610–4630.
164 J. Wu, C. Z. Liang, A. Naderi and T. S. Chung, *Adv. Materials*, 2021, 2105156.
165 G. M. Shi, H. Chen, Y. Jean and T. S. Chung, *Polymer*, 2013, **54**, 774–783.
166 T. X. Yang and T. S. Chung, *J. Mater. Chem. A*, 2013, **1**, 6081–6090.
167 T. X. Yang, G. M. Shi and T. S. Chung, *Adv. Energy Mater.*, 2012, **2**, 1358–1367.
168 M. Etxeberria-Benavides, T. Johnson, S. Cao, B. Zornoza, J. Coronas, J. Sanchez-Lainez, A. Sabetghadam, X. Liu, E. Andres-Garcia, F. Kapteijn, J. Gascon and O. David, *Sep. Purif. Technol.*, 2020, **237**, 116347.
169 V. Giel, M. Perchacz, J. Kredatusová and Z. Pientka, *Nanoscale Res. Lett.*, 2017, **12**(1), 1–15.
170 L. Cseri, R. Hardian, S. Anan, H. Vovusha, U. Schwingenschlögl, P. M. Budd, K. Sada, K. Kokado and G. Szekely, *J. Mater. Chem. A*, 2021, **9**(42), 23793–23801.
171 F. S. Model and L. A. Lee, in *Reverse Osmosis Membrane Reserach*. Springer, Boston, MA, 1972.
172 F. S. Model and L. A. Lee, *Org. Coat. Plast. Chem.*, 1972, **32**, 383.
173 M. J. Ram, *US Pat.*, 3851025, 1974.
174 L. C. Sawyer and R. S. Jones, *J. Membr. Sci.*, 1984, **20**, 147–166.
175 M. Senoo, S. Hara and S. Ozawa, *US Pat.*, 3951920, 1976.
176 H. J. Davis and J. W. Soehngen, *Chlorine Resistant PBI RO Permselective 173membranes*. A technical report of Celanese Research Co., Summit, N.J. USA, 1981.
177 F. S. Model, H. J. Davis and J. E. Poist. in *Reverse Osmosis and Synthetic Membranes-Theory, Technology, Engineering*, ed. S. Sourirajan, National Research Council, Ottawa, Canada, 1977, pp. 231–248.
178 X. Wang, P. Jayaweera, R. A. Alrasheed, S. A. Aljlil, Y. M. Alyousef, M. Alsubaei, H. Alromaih and I. Jayaweera, *Membranes*, 2018, **8**, 113.
179 M. D. Wales, E. Gebremichael, X. Wang, E. Perea, P. Jayaweera and I. Jayaweera, *Membranes*, 2021, **11**(6), 430.
180 J. E. Cadotte, *US Pat.*, 4039440, 1977.
181 R. J. Petersen, *J. Memb. Sci.*, 1993, **83**, 81–150.
182 L. P. Raman, M. Cheryan and N. Rajagopalan, *Chem. Eng. Prog.*, 1994, **90**, 68–74.
183 A. Fane, A. Schaefer and T. Waite, *Nanofiltration, Principles and Applications*. Elsevier Science, Oxford, UK, 2004.
184 I. C. Escobar, B. Van der Bruggen, *Modern Applications in Membrane Science and Technology*, American Chemical Society Books, USA, 2011.
185 K. Boussu, B. Van der Bruggen, A. Volodin, C. Van Haesendonck, J. A. Delcour, P. Van der Meeren and C. Vandecasteele, *Desalination*, 2006, **191**, 245–253.
186 F. G. Donnan, *J. Memb. Sci.*, 1995, **100**, 45–55.
187 A. E. Yaroshchuk, *Membr. Tech.*, 1998, **100**, 9–12.
188 K. D. Kreuer, A. Fuchs, M. Ise, M. Spaeth and J. Maier, *Electrochim. Acta*, 1998, **43**, 1281–1288.
189 K. Y. Wang and T. S. Chung, *J. Memb. Sci.*, 2006, **281**, 307–315.
190 K. Y. Wang, T. S. Chung and R. Rajagopalan, *Ind. Eng. Chem. Res.*, 2007, **46**, 1572–1577.
191 W.-P. Zhu, S.-P. Sun, J. Gao, F.-J. Fu and T. S. Chung, *J. Memb. Sci.*, 2014, **456**, 117–127.
192 K. Y. Wang, T. S. Chung and J. J. Qin, *J. Memb. Sci.*, 2007, **300**, 6–12.
193 M. F. Flanagan and I. C. Escobar, *J. Membr. Sci.*, 2013, **434**, 85–92.
194 S. Daer, N. Akther, Q. Wei, H. K. Shon and S. W. Hasan, *Desalination*, 2020, **491**, 114441.
195 F.-J. Fu, S. Zhang and T. S. Chung, *Desalination*, 2015, **376**, 73–81.
196 S. C. Chen, X. Z. Fu and T. S. Chung, *Desalination*, 2014, **335**, 17–26.
197 P. Vandezande, L. E. M. Gevers and I. F. J. Vankelecom, *Chem. Soc. Rev.*, 2008, **37**, 365–405.
198 E. M. Rundquist, C. J. Pink and A. G. Livingston, *Green Chem.*, 2012, **14**, 2197–2205.
199 X. Q. Cheng, Y. L. Zhang, Z. X. Wang, Z. H. Guo, Y. P. Bai and L. Shao, *Adv. Polym. Technol.*, 2014, **33**, 1–24.
200 G. Szekely, M. F. Jimenez-Solomon, P. Marchetti, J. F. Kim and A. G. Livingston, *Green Chem.*, 2014, **16**, 4440–4473.
201 P. Marchetti, M. F. Jimenez Solomon, G. Szekely and A. G. Livingston, *Chem. Rev.*, 2014, **114**, 10735–10806.
202 G. M. Shi, Y. Feng, B. Li, H. M. Tham, J.-Y. Lai and T. S. Chung, *Prog. Polym. Sci.*, 2021, **123**, 101470.
203 S. Sourirajan, *Nature*, 1964, **203**, 1348–1349.
204 L. S. White and A. R. Nitsch, *J. Memb. Sci.*, 2000, **179**, 267–274.
205 C. Didaskalou, J. Kupai, L. Cseri, J. Barabas, E. Vass, T. Holtzl and G. Szekely, *ACS Catal.*, 2018, **8**(8), 7430–7438.
206 H. M. Tham, K. Y. Wang, D. Hua, S. Japip and T. S. Chung, *J. Memb. Sci.*, 2017, **542**, 289–299.
207 H. M. Tham and T. S. Chung, *J. Memb. Sci.*, 2020, **610**, 118294.
208 S. Darvishmanesh, F. Tasselli, J. C. Jansen, E. Tocci, F. Bazzarelli, P. Bernardo, P. Luis, J. Degrève, E. Drioli and B. Van der Bruggen, *J. Memb. Sci.*, 2011, **384**, 89–96.
209 M. H. D. A. Farahani and T. S. Chung, *Chem. Eng. J.*, 2018, **345**, 174–185.
210 H. Y. Jang, J. R. Johnson, Y. Ma, R. Mathias, D. A. Bhandari and R. P. Lively, *AIChE J*, 2019, **65**, 16757.
211 B. Li, S. Japip, J.-Y. Lai and T. S. Chung, *Chem. Eng. J.*, 2021, **422**, 130015.
212 K. Y. Wang, B. Li and T. S. Chung, *J. Memb. Sci.*, 2021, **638**, 119678.
213 R. Y. M. Huang, *Pervaporation Membrane Separation Processes*, Elsevier Science Publishers B.V., 1991.
214 G. Liu and W. Jin, *J. Memb. Sci.*, 2021, **636**, 119557.
215 Y. K. Ong, G. M. Shi, L. Le Ngoc, Y. P. Tang, J. Zuo, S. P. Nunes and T. S. Chung, *Prog. Polym. Sci.*, 2016, **57**, 1–31.

216 Y. Wang, *Ind. Eng. Chem. Res.*, 2015, **54**, 3082–3089.
217 W. J. Koros and G. K. Fleming, *J. Memb. Sci.*, 1993, **83**, 1–80.
218 K. Ghosal and B. D. Freeman, *Polym. Adv. Technol.*, 1994, **5**, 673–697.
219 L. M. Robeson, *Curr. Opin. Solid State Mater. Sci.*, 1999, **4**, 549–552.
220 C. Z. Liang, T. S. Chung and J.-Y. Lai, *Prog. Polym. Sci.*, 2019, **97**, 101141.
221 H. Lin, E. Van Wagner, B. D. Freeman, L. G. Toy and R. P. Gupta, *Science*, 2006, **311**, 639–642.
222 J. D. Perry, K. Nagai and W. J. Koros, *MRS Bull.*, 2006, **31**, 745–749.
223 L. Shao, B. T. Low, T. S. Chung and A. R. Greenberg, *J. Membr. Sci.*, 2009, **327**, 18–31.
224 A. X. Y. Mah, W. S. Ho, C. P. C Bong, M. H. Hassim, P. Y. Liew, U. A. Asli, M. J. Kamaruddin and N. G. Chemmangattuvalappil, *Int. J. Hydrogen Energy*, 2019, **44**, 5661–5675.
225 N. W. Ockwig and T. M. Nenoff, *Chem. Rev.*, 2007, **107**, 4078–4110.
226 S. P. Cardoso, I. S. Azenha, Z. Lin, I. Portugal, A. E. Rodrigues and C. M. Silva, *Sep. Purif. Rev.*, 2018, **47**, 229–266.
227 R. W. Baker, *Ind. Eng. Chem. Res.*, 2002, **41**, 1393–1411.
228 G. Krishnan, D. Steele, K. O'Brien, R. Callahan, K. Berchtold and J. Figueroa, *Energy Procedia*, 2009, **1**, 4079–4088.
229 D. R. Pesiri, B. Jorgensen and R. C. Dye, *J. Memb. Sci.*, 2003, **218**, 11–18.
230 S. D. Kenarsari, D. Yang, G. Jiang, S. Zhang, J. Wang, A. G. Russell, Q. Wei and M. Fan, *RSC Adv.*, 2013, **3**, 22739–22773.
231 H. S. Lau and W. F. Yong, *J. Mater. Chem. A*, 2021, **9**, 26454–26497.
232 S. C. Kumbharkar and K. Li, *J. Memb. Sci.*, 2012, **415**, 793–800.
233 K. A. Berchtold, R. P. Singh, J. S. Young and K. W. Dudeck, *J. Memb. Sci.*, 2012, **415**, 265–270.
234 J. Sánchez-Laínez, M. Etxeberria-Benavides, O. David, C. Téllez and J. Coronas, *ChemSusChem*, 2021, **14**, 952–960.
235 A. Naderi, T. S. Chung, M. Weber and C. Maletzko, *J. Memb. Sci.*, 2019, **591**, 117292.
236 L. F. Villalobos, R. Hilke, F. H. Akhtar and K. V. Peinemann, *Adv. Energy Mater.*, 2018, **8**, 1701567.
237 D. Y. Kim, S. Ryu, H. Kim, H. C. Ham, H. Sohn, S. P. Yoon, J. Han, T. Lim, J. Y. Kim, S. W. Lee, C. W. Yoon and S. H. Choi, *Sep. Purif. Technol.*, 2021, **257**, 117954.
238 B. W. Rowe, L. M. Robeson, B. D. Freeman and D. R. Paul, *J. Memb. Sci.*, 2010, **360**, 58–69.
239 J. R. Klaehn, C. J. Orme and E. S. Peterson, *J. Memb. Sci.*, 2016, **515**, 1–6.
240 J. Wu and T. S. Chung, *Small Methods*, 2021, 2101288.
241 B. P. Biswal, A. Bhaskar, R. Banerjee and U. K. Kharul, *Nanoscale*, 2015, **7**, 7291–7298.
242 A. Kumar, L. Huang, L. Hu, D. Yin, H. Lin and M. T. Swihart, *J. Mater. Chem. A*, 2021, **9**(21), 12755–12762.
243 A. S. Rewar, R. S. Bhavsar, K. Sreekumar and U. K. Kharul, *J. Membr. Sci.*, 2015, **481**, 19–27.
244 M. Omidvar, H. Nguyen, L. Huang, C. M. Doherty, A. J. Hill, C. M. Stafford, X. Feng, M. T. Swihart and H. Lin, *ACS Appl. Mater. Interfaces*, 2019, **11**, 47365–47372.
245 J. G. Seong, J. C. Lewis, J. A. Matteson, E. Craddock, U. Martinez, H. Thakkar, A. D. Benavidez, K. A. Berchtold and R. P. Singh, *Carbon*, 2022, **192**, 71–83.
246 *Materials Science of Membranes for Gas and Vapor Separation*. ed. B.D. Freeman and Y. Yampolskii, I. Pinnau, John Wiley & Sons, 2006.
247 N. Iwamoto, *Polym. Eng. Sci.*, 1994, **34**, 434–437.
248 J. Liu, X. Kong and J. Jiang, *J. Memb. Sci.*, 2018, **564**, 782–787.
249 J. Liu and J. Jiang, *Polymer*, 2019, **185**, 121932.

